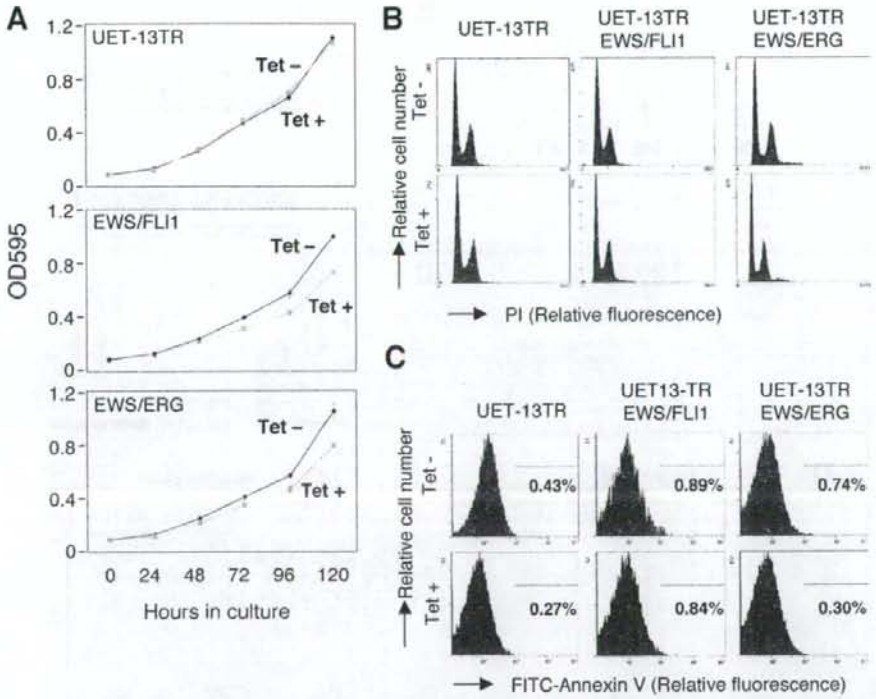

FIG. 2. Effects of EWS/ETS on cell growth in UET-13 cells. (A) Growth curve for UET-13 transfectants. Cells were seeded at 10^5/well and cultured as described for Fig. 1. The increase in cell number was analyzed by MTT assay. Values are means with the standard errors (SE) from three independent experiments. Diamond symbols indicate UET-13 transfectants in the absence of tetracycline (Tet); box symbols indicate UET-13 transfectants in the presence of tetracycline. (B) Cells were cultured as described for panel A in the absence or presence of tetracycline for 3 days and then stained with PI, and DNA contents were analyzed by flow cytometry (*x* axis, relative intensity of fluorescence; *y* axis, relative cell number). (C) Cells treated as described for panel B were stained with FITC-annexin V and analyzed.

Microarray data accession numbers. Microarray data have been deposited in the Gene Expression Omnibus database GEO (www.ncbi.nlm.nih.gov/geo) (accession numbers GSE8665 and GSE8596).

RESULTS

EWS/ETS expression results in morphological changes in UET-13 cells. To investigate how the expression of EWS/ETS affects human MPCs, we used UET-13 cells as a model of human MPCs and expressed EWS/FLI1 (UET-13TR-EWS/FLI1) and EWS/ERG (UET-13TR-EWS/ERG) in a tetracycline-inducible manner (Fig. 1A). As shown in Fig. 1B and C, we confirmed that the tetracycline treatment could induce EWS/ETS expression by RT-PCR analysis and Western blotting. The inducibility upon the addition of doxycycline was comparable to that upon the addition of tetracycline.

Using these cell systems, first we examined the effect of EWS/ETS expression on morphology in UET-13 transfectants. When tetracycline was added to the culture, the morphologies of both UET-13TR-EWS/FLI1 and UET-13TR-EWS/ERG cells were dramatically changed (Fig. 1D). Tetracycline-treated UET-13TR-EWS/ETS cells consisted of a mixture of small round-to-polygonal cells and short spindle cells. The cell morphology resembled that of EFT cell lines. To assess the reproducibility of this phenotypic change, other UET-13TR-EWS/ETS clones were examined, and similar morphological changes were observed. Since tetracycline treatment did not affect the morphology of UET-13TR cells (Fig. 1D), it was suggested that the morphological alteration in UET-13 cells from a mesenchymal cell shape to small round cells, one of the characteristics of EFT, can be attributed to EWS/ETS expression.

EWS/ETS expression inhibits cell growth in UET-13 cells. Next, the effect of EWS/ETS expression on the growth of UET-13 cells was analyzed. As shown in Fig. 2A, an MTT assay revealed that the addition of tetracycline had no effect on the growth of UET-13TR cells but slightly inhibited that of UET-13TR-EWS/ETS cells. We also assessed the cell growth of UET-13 transfectants after tetracycline addition by cell counting and obtained results well in accord with those from the MTT assay (data not shown). To determine the mechanism of this inhibition, DNA content and the binding of annexin V to UET-13 transfectants were examined. No significant increase in either sub-G_1-phase cells (Fig. 2B) or annexin V binding cells (Fig. 2C) was detected, suggesting that EWS/ETS-mediated growth inhibition in UET-13 cells was not due to the activation of an apoptotic pathway. Moreover, no significant decrease in S-G_2-phase cells was observed (Fig. 2B).

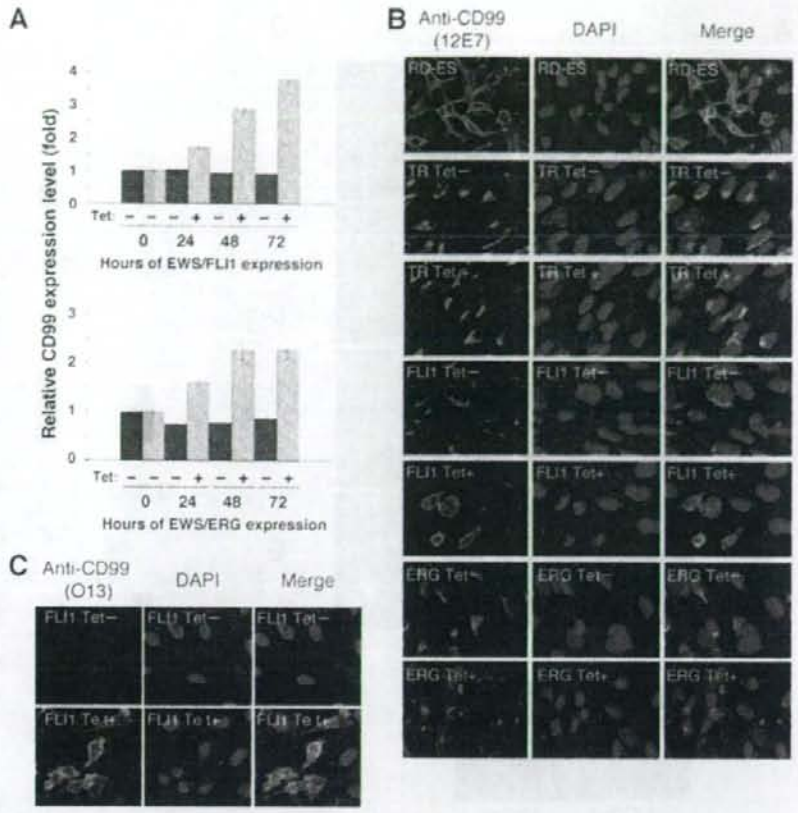

FIG. 3. Effects of tetracycline-mediated EWS/ETS expression on the expression and distribution of CD99 in UET-13 cells. (A) Relative CD99 levels in UET-13 transfectants in the absence or presence of tetracycline (Tet). UET-13 transfectants were treated with or without 3 μg/ml of tetracycline for the indicated periods. Real-time RT-PCR was performed to investigate the expression pattern of CD99. Signal intensities of CD99 were normalized using those of a control housekeeping gene (human GAPDH gene). Data are relative values with standard deviations from triplicate wells and are normalized to the mRNA level at 0 h, which is arbitrarily set to 1 in the graphical presentation. (B and C) Immunocytostaining of CD99 in UET-13 transfectants. Cells were cultured on coverslips in the absence or presence of tetracycline for 72 h and then stained with anti-CD99 antibody 12E7 (B) or O13 (C) as described in Materials and Methods. RD-ES cells were also examined as a positive control. For the staining of nuclei, DAPI was used.

Effect of EWS/ETS on CD99 expression in UET-13 cells. The p30/32MIC-2 gene product, CD99, is a cell surface glycoprotein expressed in EFT with a strong membranous staining pattern and thus constitutes a useful marker for EFT (2, 30). Knowing the dramatic change of morphology in UET-13 cells, we next investigated the mRNA level of CD99 in tetracycline-treated and untreated UET-13 transfectants by quantitative real-time RT-PCR. CD99 levels were clearly elevated by tetracycline treatment in both UET-13TR-EWS/FLI1 and UET-13TR-EWS/ERG cells in a time-dependent manner (Fig. 3A).

We also examined the protein expression of CD99 by immunostaining using 12E7 antibody, which is most widely used as an anti-CD99 antibody. An EFT cell line, RD-ES, showed strong membranous staining of CD99 (Fig. 3B), while neither UET-13TR cells nor UET-13 cells had such a staining. Of note is the fact that although 12E7 reactivity was observed only in the cytoplasm in perinuclear regions in both UET-13TR (Fig. 3B) and UET-13 (data not shown) cells, this antibody is well known to cross-react with a cytoplasmic protein not yet characterized. Since another anti-CD99 antibody, O13, did not react with either UET-13TR (Fig. 3C) or UET-13 (data not shown) cells, we concluded that the perinuclear staining of 12E7 mentioned above was a cross-reaction with unrelated proteins.

In the absence of tetracycline, both UET-13TR-EWS/FLI1 and UET-13TR-EWS/ERG cells were also negative with anti-CD99 antibodies (a pattern designated $CD99^-$), similar to UET-13 cells. Surprisingly, however, tetracycline induced a membranous staining pattern (designated $CD99^+$) in UET-13TR-EWS/FLI1 and UET-13TR-EWS/ERG cells, and some $CD99^+$ cells had irregularly contoured nuclei (Fig. 3B). The same results were observed with another anti-CD99 antibody, O13 (Fig. 3C), indicating that the membranous staining observed for UET-13 transfectants with the anti-CD99 antibodies

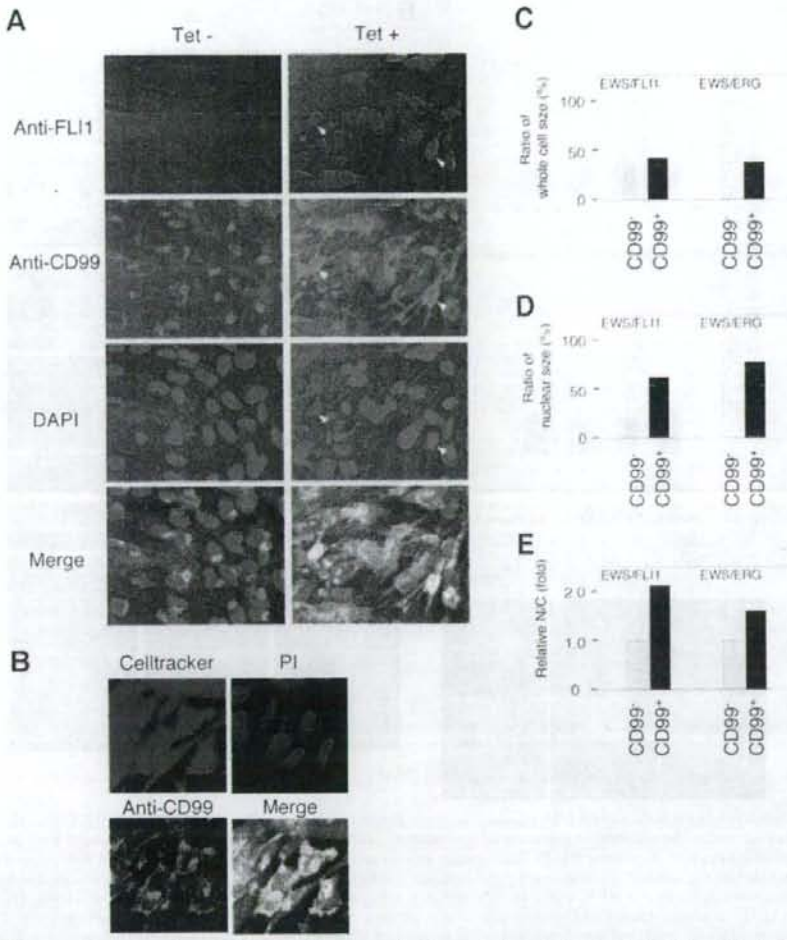

FIG. 4. EWS/ETS expression, alteration of CD99 distribution, and cell morphological changes in UET-13 cells. (A) Immunofluorescence studies using anti-Fli1 (red), anti-CD99 (green), and DAPI (blue). UET-13TR-EWS/FLI1 cells were cultured on coverslips in the absence or presence of tetracycline (Tet) for 72 h and then stained as described in Materials and Methods. White arrowheads indicate $CD99^+$ cells that have a strong staining pattern with anti-Fli1 antibodies and also have remarkable CD99 expression and morphological features. (B) Immunofluorescence analysis by triple staining with whole cells (Celltracker; blue), CD99 (anti-CD99; green), and nuclei (PI; red). UET-13TR-EWS/FLI1 cells were cultured as described for panel A and then stained as described in Materials and Methods. (C to E) Measurements of whole-cell size (C), nuclear size (D), and N/C ratio (E) in tetracycline-treated UET-13 transfectants. UET-13TR-EWS/FLI1 and UET-13TR-EWS/ERG cells were cultured on coverslips in the presence of tetracycline for 72 h and then stained as described in Materials and Methods. These samples were analyzed by the image analysis software Image J ($n = 50$). (C and D) Data are relative values with the SE and are normalized to the size of $CD99^-$ cells, which is arbitrarily set to 100. (E) Data are relative values with the SE and are normalized to the size of $CD99^-$ cells, which is arbitrarily set to 1.

was really CD99 derived. Despite the fact that cells were single colony derived, there was a heterogeneous response to tetracycline treatment in UET-13TR-EWS/FLI1 and UET-13TR-EWS/ERG cells, but most of the $CD99^+$ cells had a small round morphology, one of the characteristics of EFT. To assess the correlation between EWS/FLI1 expression and the change of the CD99 expression pattern, we performed immunofluorescence studies using anti-Fli1 and anti-CD99 antibodies. As shown in Fig. 4A, tetracycline treatment induced a marked enhancement of nuclear staining with anti-Fli1 antibodies in a large number of UET-13TR-EWS/FLI1 cells, indicating the induction of EWS/FLI1 proteins. Furthermore, we observed that the cells with a strong signal for Fli1 tended to reveal a membranous staining pattern with anti-CD99 antibodies and a small round morphology (Fig. 4A). To further verify the correlation between CD99 expression pattern and cell morphology, we estimated the size of cells by triple staining using Celltracker Blue, PI, and anti-CD99 antibody (Fig. 4B). As

TABLE 2. Immunophenotypic characterization of UET-13 transfectants and EFT cells

MPC status[a]	CD marker	Result for[b]: UET-13	UET-13TR		UET-13TR-EWS/FLI1		UET-13TR-EWS/ERG		RD-ES	EFT status[c]	SK-ES1
		Tet⁻	Tet⁻	Tet⁺	Tet⁺	Tet⁻	Tet⁺				
M+	CD29	+	+	+	+	+	+	+	+	+	
M+	CD59	+	+	+	+	+	+	+	+	+	
M+	CD90	+	+	+	+	+	+	+	+	+	E+
M+	CD105	+	+	+	+	+	+	+	+	+	
M+	CD166	+	+	+	+	+	+	+	+	+	
M+	CD44	+	+	+	+	+	+	+	−	−	
M+	CD73	+	+	+	+	+	+	+	−	−	
M+	**CD10**	+	+	+	+	**Down**	+	**Down**	−	−	
M+	**CD13**	+	+	+	+	**Down**	+	**Down**	−	−	
M+	**CD49e**	+	+	+	+	**Down**	+	**Down**	+	−	
M+	**CD61**	+	+	+	+	**Down**	+	**Down**	−	−	
M+	**CD55**	+	+	+	+	**Down**	+	+	+	−	
M+	**CD54**	−	−	−	−	**Up**	−	**Up**	+	+	E+
M(−)	**CD117**	−	−	−	−	**Up**	−	**Up**	+	+	E+
M+/−	**CD271**	−	−	−	−	**Up**	−	**Up**	+	+	E+
	CD40	−	−	−	−	−	−	−	+	+	E+
	CD56	−	−	−	−	−	−	−	+	+	E+
M(−)	CD133	−	−	−	−	−	−	−	+	+	
M(−)	CD14	−	−	−	−	−	−	−	−	−	
M(−)	CD34	−	−	−	−	−	−	−	−	−	
M(−)	CD45	−	−	−	−	−	−	−	−	−	

[a] M(−), negative for MPCs; M+/−, positive for BM-derived MPCs but negative after in vitro culture; M+, positive for MPCs.
[b] +, most cells positive; −, negative; Up, up-regulated by tetracycline treatment; Down, down-regulated by tetracycline treatment. Boldface indicates the antigens the immunophenotypes of which were changed in favor of EFT. Tet⁻, tetracycline negative; Tet⁺, tetracycline positive.
[c] E+, positive for EFTs.

presented in Fig. 4C and D, the results clearly showed that the majority of CD99⁺ cells were significantly smaller in both whole-cell size and nuclear size than the CD99⁻ cells. Moreover, CD99⁺ cells also had a substantially increased N/C ratio (Fig. 4E). These results indicated that EWS/ETS expression promoted CD99 expression in UET-13 cells, and CD99 expression status is correlated with the degree of morphological change.

EWS/ETS expression altered the immunophenotype of UET-13 cells. Human MPCs reveal a characteristic expression of several surface antigens and can be identified on the basis of the reactivity with a set of monoclonal antibodies against CD antigens (25, 42). On the other hand, some CD antigens are characteristically expressed on EFT cells (17, 28, 33). Using the combinations of these antibodies listed in Table 2, which are useful for the immunodetection of either MPCs or EFT cells, we further examined whether EWS/ETS expression affects the immunophenotype of UET-13 cells and compared its effect with that on the immunophenotype of EFT cell lines (Table 2 and Fig. 5). As shown in Table 2, UET-13 cells express most of the human primary MPCs markers. Some of the antigens expressed in MPCs, namely, CD29, CD59, CD90, CD105, and CD166, were also found to be expressed in EFT cell lines, but others, namely, CD10, CD13, CD44, CD61, and CD73, were not. In contrast, antigens recognized to be present in EFT cells, including CD40, CD56, and CD133, were absent from UET-13 cells. Interestingly, when the effect of tetracycline-mediated EWS/ETS expression on the immunophenotype of UET-13 cells was tested, levels of some of the antigens present in UET-13 cells, such as CD10, CD13, and CD61, were found to be decreased (Fig. 5). In contrast, some of the markers found in EFT cells, i.e., CD54, CD117, and CD271, became positive in UET-13TR-EWS/ETS cells after tetracycline treatment. Because UET-13TR cells did not show such immunophenotypic change upon treatment with tetracycline, these results indicated that, at least in part, the immunophenotype of UET-13 cells was changed in favor of EFT in the presence of EWS/ETS.

EWS/ETS in UET-13 cells modulates EFT-like gene expression. To further examine the molecular mechanism of EWS/ETS-dependent cellular modulation in human mesenchymal progenitor background, we performed DNA microarray-based expression profiling using the Affymetrix human genome U133 Plus 2.0 array. As a first step to this approach, we validated our experimental systems by analyzing the sequential changes of known EWS/ETS target genes, i.e., inhibitor of differentiation 2 (ID2) (14, 39), NK2 transcription factor related, locus 2 (NKX2.2) (9, 48), and insulin-like growth factor binding protein 3 (IGFBP3) (41). Consistent with previous reports, levels of ID2 and NKX2.2 increased with the expression of EWS/ETS in a time-dependent manner, whereas the expression level of IGFBP3 decreased (Fig. 6A). Employing the same procedure, we also examined whether the change of surface antigen expression was regulated at the transcriptional level and determined the mRNA expression levels of some surface antigens in UET-13 transfectants with or without tetracycline treatment. In accordance with the results of immunocytometric and immunohistological experiments, the mRNA expression levels of CD10, CD13, CD49e, and CD61 were decreased, while those of CD54, CD99, CD117, and CD271 were markedly increased in tetracycline-treated UET-13TR-EWS/ETS cells (Fig. 6B and C), indicating that the expression of these antigens is

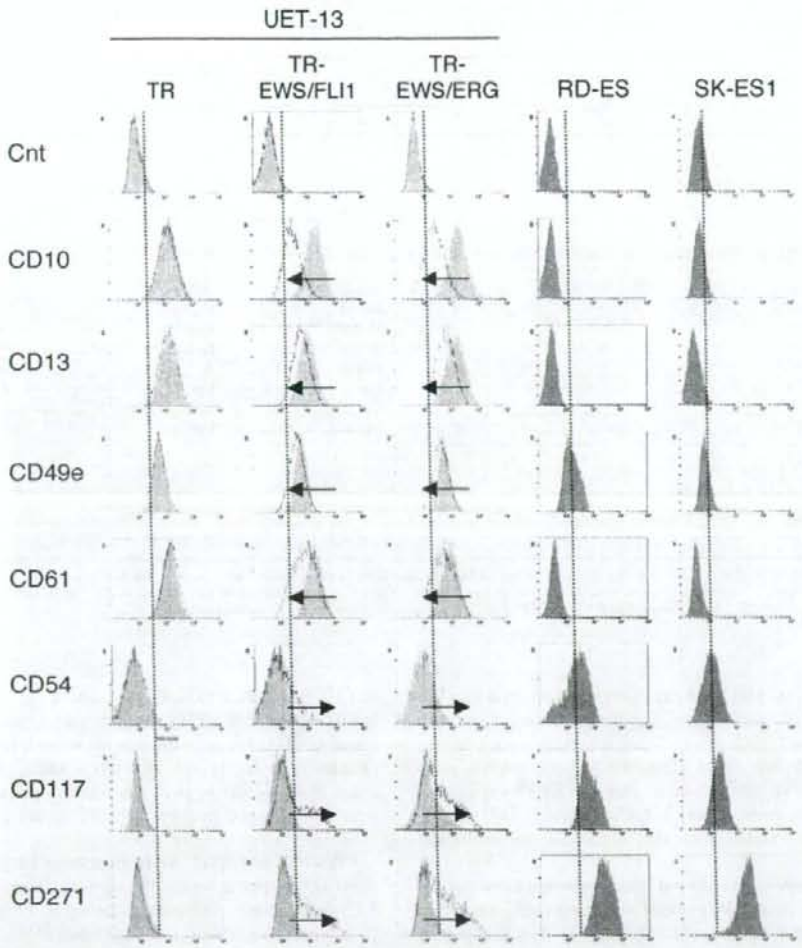

FIG. 5. Immunophenotypic change on induction of EWS/ETS expression in UET-13 cells. UET-13 transfectants were cultured with or without 3 μg/ml of tetracycline for 1 week and flow cytometric analyses were performed by using a set of antibodies as indicated. The histograms of UET-13 transfectants with (empty) and without (gray) tetracycline treatment were overlaid. Dotted lines indicate fluorescence intensities in negative control panels (Cnt). Arrows indicate the immunophenotypic change caused by tetracycline. The immunophenotypes of the EFT cell lines RD-ES and SK-ES1 were also examined.

controlled at the transcriptional level in the presence of EWS/ETS.

We next investigated the candidate genes whose expression is regulated by EWS/ETS in human MPCs. First, we selected the genes with up-regulated or down-regulated expression by EWS/ETS induction using gene cluster analysis (Fig. 7A; UET-13TR-EWS/FLI1 up, 4,294 probes; down, 4,103 probes; UET-13TR-EWS/ERG up, 3,358 probes; down, 3,705 probes). To reduce the number of the candidate genes, we selected up-regulated genes that are expressed in tetracycline-treated cells at least 1.5-fold higher than in untreated cells (UET-13TR-EWS/FLI1, 1,137 probes; UET-13TR-EWS/ERG, 835 probes). Similarly, the down-regulated genes that are expressed in tetracycline-treated cells at least 0.75-fold lower than in untreated cells (UET-13TR-EWS/FLI1, 1,803 probes; UET-13TR-EWS/ERG, 773 probes). By selecting common probes in both cells, we finally identified a group of candidate genes significantly controlled by EWS/ETS induction in the human mesenchymal progenitor background. Since microarray analysis was performed as a global screening in a single experiment, it is likely that there is a fair bit of noise in the derived gene profiles due to the lack of replicate data. This may account in part for the limited overlap between the profiles induced by EWS-FLI1 and EWS-ERG, whereas we still identified 349 probes of common up-regulated genes and 293 probes of common down-regulated genes (see the supplemental material). In addition to the EFT-specific genes mentioned above, these contained those previously described as EFT-specific genes, such as those for OB-cadherin/cadherin-11 (31), Janus

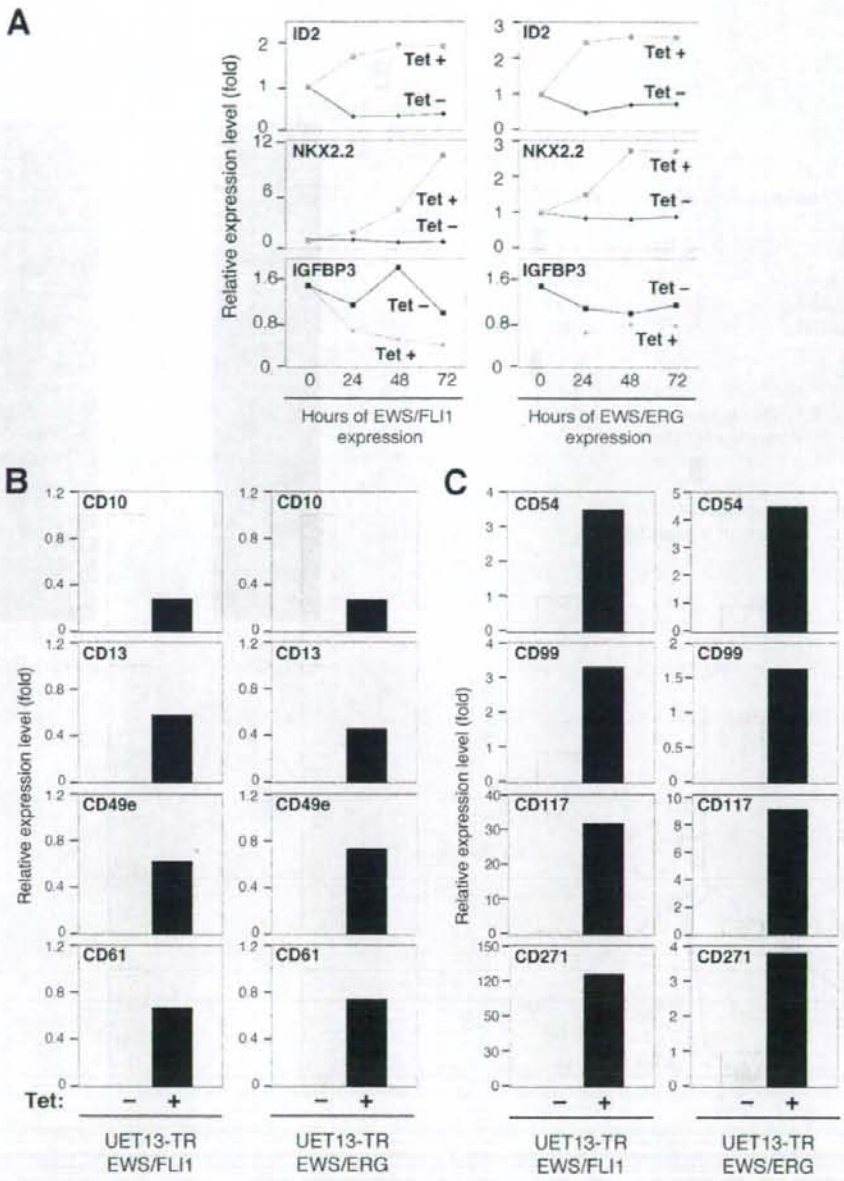

FIG. 6. The change of expression profile on induction of EWS/ETS in UET-13 cells. UET-13TR-EWS/FLI1 and UET-13TR-EWS/ERG cells were cultured in the absence or presence of tetracycline (Tet) for the indicated periods and analyzed using the Affymetrix human genome U133 Plus 2.0 array as described in Materials and Methods. (A) The sequential changes of ID2, NKX2.2, and IGFBP3 mRNA levels in UET-13 transfectants upon treatment with or without tetracycline. Diamond symbols indicate UET-13 transfectants in the absence of tetracycline; box symbols indicate UET-13 transfectants in the presence of tetracycline. (B and C) Microarray studies for the determination of expression profiles of surface antigens in UET-13 transfectants. UET-13 transfectants were treated with or without 3 μg/ml of tetracycline for 72 h. mRNA levels were determined with the Affymetrix human genome U133 Plus 2.0 array.

kinase 1 (JAK1) (49), keratin 18, and six-transmembrane epithelial antigen of the prostate (STEAP) (22). The expression pattern of these genes (642 probes) in UET-13 transfectants in the absence or presence of tetracycline is shown in the gene cluster in Fig. 7B. The expression of these genes was indeed changed significantly after EWS/ETS expression in both cells. They included genes associated with signal transduction (such as those for epidermal growth factor receptor, FAS [CD95], and fibroblast

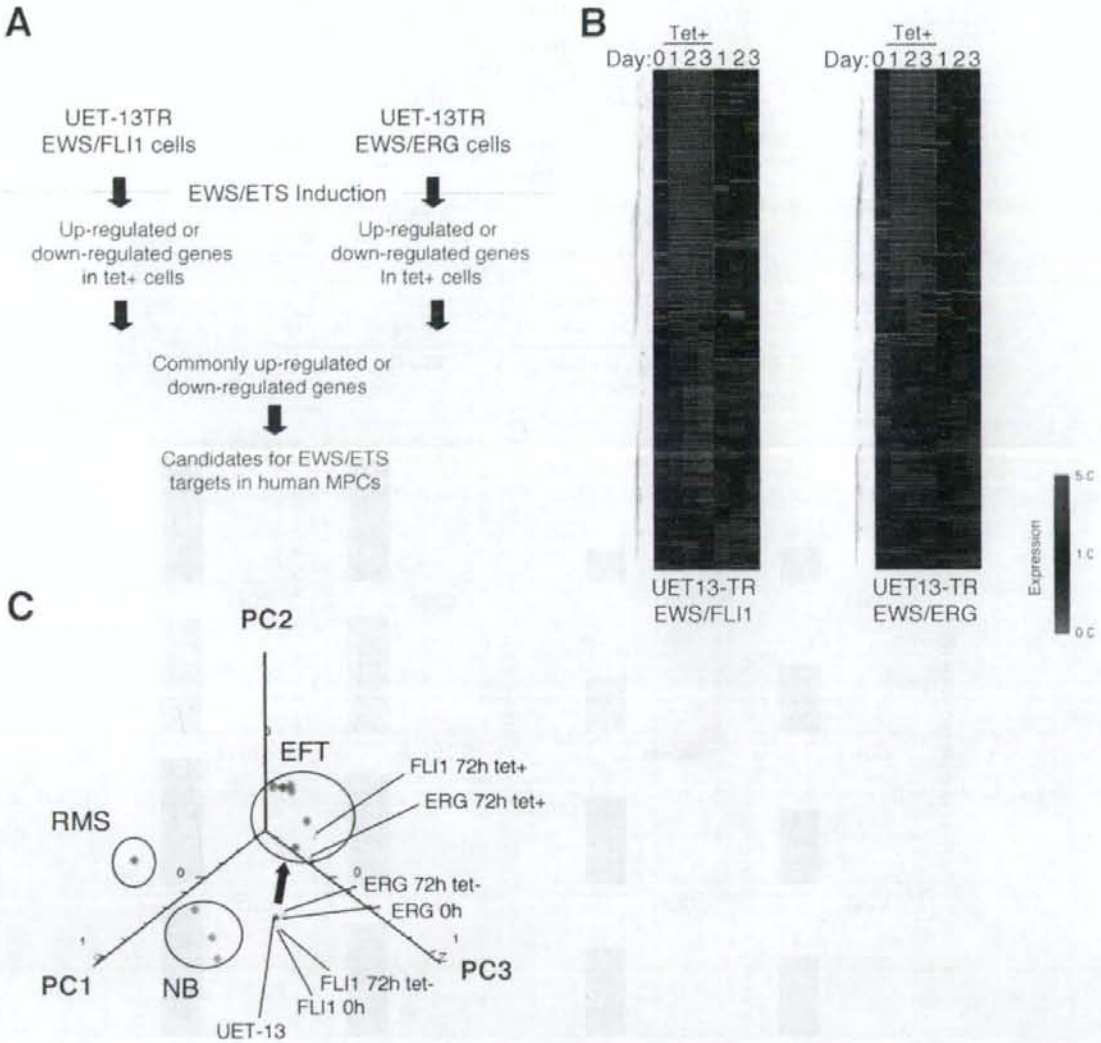

FIG. 7. Identification of candidates for the target of EWS/ETS in human MPCs by use of a microarray. UET-13TR-EWS/FLI1 and UET-13TR-EWS/ERG cells were cultured as described for Fig. 6 and analyzed using the Affymetrix human genome U133 Plus 2.0 array as described in Materials and Methods. (A) Scheme for the analysis of microarray data. (B) Gene cluster analysis of UET-13 transfectants in the absence or presence of tetracycline by use of 642 candidate genes for targets of EWS/ETS in human MPCs. (C) Visualization of sequential change by the gene expression profile in UET-13 transfectants following tetracycline-mediated EWS/ETS expression based on a PCA of 642 candidate genes. Deep blue plots indicate UET-13 cells. Light blue plots indicate UET-13 transfectants in the absence of tetracycline for 72 h. Yellow plots indicate UET-13 transfectants in the presence of tetracycline for 72 h. The pink circle indicates EFT cell lines expressing EWS/FLI1 (purple plots), EWS/ERG (red plot), and EWS/E1AF (light green plot). The light blue circle with blue plots indicates NB cell lines. The yellow circle with an orange plot indicates a rhabdomyosarcoma (RMS) cell line. Cutoff induction and repression levels are 1.5-fold and 0.75-fold, respectively. Tet, tetracycline.

growth factor receptor 1) and development (such as jagged-1 and frizzled-4, -7, and -8). Interestingly, in addition to the surface antigens presented in Fig. 6B and C, the expression profiling of EWS/ETS-expressing UET-13 cells displayed the modulation of several genes associated with cell adhesion, cytoskeletal structure, and membrane trafficking, such as those for collagen-11 and -21, ephrin receptor-A2, -B2, and -B3, ephrin-B1, claudin-1, integrin-α11, -αM, and -β2, CD66 (carcinoembryonic antigen-related cell adhesion molecule-1), and CD102 (intercellular cell adhesion molecule-2). They also included genes of chemokines CCL-2 and -3. These data raise the possibility that EWS/ETS can contribute to the membrane condition in human MPCs via the regulation of these cell surface molecules and chemokines.

Using these genes, we performed a PCA to visualize the shift in the gene expression pattern among the 642 probes. As shown in Fig. 7C, the plots of UET-13 transfectants treated with tetracycline became closer to those of EFT cells than to those of UET-13 transfectants without tetracycline treatment. These results indicated that the expression pattern of these genes was altered from that of UET-13 cells to that of EFT cells in an EWS/ETS-dependent manner. Since the gene expression profile of UET-13 cells is similar to those of other cell types of mesenchymal origin (data not shown), our results highlighted that the phenotypic alteration from mesenchyme to EFT-like cells in UET-13 cells induced by tetracycline treatment was accompanied by a change in the global gene expression profile.

EWS/ETS expression enhances the Matrigel invasion of UET-13 cells. To assess the role of EWS/ETS in malignant transformation in human MPCs, UET-13 transfectants were examined by invasion assay. As shown in Fig. 8A, tetracycline treatment did not affect the Matrigel invasion ability of UET-13TR cells. When examined similarly, however, tetracycline treatment resulted in an apparently increased invasion ($P < 0.05$) for both UET-13TR-EWS/FLI1 (Fig. 8B) and UET-13TR-EWS/ERG (Fig. 8C) cells. The results indicated that EWS/ETS expression can induce Matrigel invasion properties in human MPCs.

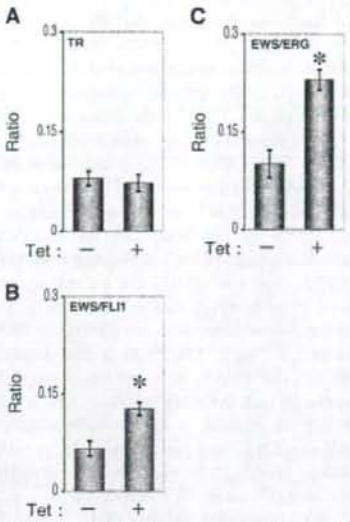

FIG. 8. Effects of EWS/ETS expression on the Matrigel invasion ability of UET-13 cells. UET-13TR (A), UET-13TR-EWS/FLI1 (B), and UET-13TR-EWS/ERG (C) cells were cultured in the absence or presence of tetracycline (Tet) for 72 h and then plated (2.5×10^4) on Matrigel-coated or uncoated filter inserts. After 20 h of culture, invading cells were stained with hematoxylin-eosin and counted in five fields per membrane as described in Materials and Methods. *, $P < 0.05$.

DISCUSSION

In the present study, using UET-13 cells as a model of human MPCs, we demonstrated that ectopic expression of EWS/ETS promoted the acquisition of an EFT-like phenotype, including cellular morphology, immunophenotype, and gene expression profile. Moreover, EWS/ETS expression enhances the ability of UET-13 cells to invade Matrigel. This assay is thought to mimic the early steps of tumor invasion in vivo (34), and the ability to penetrate the Matrigel has been positively correlated with invasion potential in several studies. Therefore, we concluded that EWS/ETS expression could mediate a part of the feature of tumor transformation in human MPCs. Thus, our culture system would provide a good model for testing the effects of EWS/ETS in human MPCs.

Several lines of evidence have indicated the transforming ability of EWS/FLI1, whereas that of EWS/ERG is not yet to be clarified. Therefore, it is noteworthy that our data demonstrated that EWS/ERG could promote an EFT-like phenotype in UET-13 cells similarly to EWS/FLI1. Thus, EWS/ERG also has the ability to induce an EFT-like phenotype in the human system. The major steps in the development of EFT should be commonly regulated by distinct chimeric EWS/ETS proteins. Indeed, several genes are common transcriptional targets of different chimeric EWS/ETS proteins in the murine system (11, 24, 35). Our data also showed that the 642 probes are coregulated in both EWS/FLI1-expressing cells and EWS/ERG-expressing cells. Further comparative studies of both the EWS/FLI1- and the EWS/ERG-mediated onset of EFT could allow us to understand the common functions of EWS/FLI1 and EWS/ERG in EFT. In addition, our systems are also useful for precisely distinguishing between the functions of these chimeric molecules in the development of EFT.

As mentioned above, the immunophenotypic analysis also revealed that the expression profiles of surface antigens in UET-13 cells were changed in favor of EFT cells in the presence of EWS/ETS (Fig. 4). Notably, the expression of CD54 (intercellular cell adhesion molecule-1 [ICAM1]), CD117 (c-kit), and CD271 (low-affinity nerve growth factor receptor [LNGFR]) increased in EWS/ETS-expressing UET-13 cells. These markers are positive in EFT cell lines (17, 28, 33), and in addition, CD117 is detected in about 40% of patient samples (17) and is negative in human primary MPCs (4, 43). Thus, it is reasonable to consider that a phenotypic marker of EFT was induced in UET-13 cells by EWS/ETS expression. On the other hand, CD54 and CD271 are positive in human primary MPCs (8, 25, 42), whereas these markers are negative in UET-13 cells. However, a previous report showed the disappearance of some positive markers, including CD271, from primary human MPCs during the process of ex vivo expansion

(25), and it has been speculated that the expression of these molecules in MPCs is induced in vivo via interaction with the bone marrow microenvironment and that the necessary stimuli are absent from ex vivo culture conditions. Therefore, the immunophenotype of UET-13 cells rather might be related to that of ex vivo-expanded primary human MPCs. In addition, it may be possible that EWS/ETS expression led to the reexpression of these disappeared markers in UET-13 cells without the necessary stimuli. In this case, the maintenance of CD271 expression outside of the bone marrow microenvironment might be a characteristic of EFT. Thus, our results proved that both EWS/FLI1 and EWS/ERG can be major causes of the expression of these markers and that human MPCs that precisely recapitulate the expression are strong candidates for the cell origins of EFT cells. The findings also imply that these antigens are suitable targets for diagnostic tools and new therapeutic agents. In fact, imatinib mesylate, which demonstrates anticancer activity against malignant cells expressing BCR-ABL as well as CD117 and platelet-derived growth factor receptor, inhibits proliferation and increases sensitivity to vincristine and doxorubicin in EFT cells (17).

Notably, our results also indicate that UET-13 cells, which have the MPC phenotype, possess the potential to acquire an EFT-like phenotype upon the expression of EWS/ETS. Unlike what is seen for human primary fibroblasts (31), ectopic EWS/ETS expression induces an EFT-like morphological change in human MPCs, suggesting that the cell type affects susceptibility to the events following EWS/ETS expression. In murine MPCs, retrovirally transduced EWS/FLI1 has been reported to induce the expression of CD99, a most useful marker for EFT, though the results are controversial (6, 45). However, our direct evidence obtained with UET-13 cells clearly demonstrated that CD99 expression is induced by EWS/ETS proteins in human MPCs. Moreover, we showed that the expression of CD99 might correlate with EWS/ETS-mediated morphological change, whereas the functional role of CD99 and the correlation between CD99 expression status and EWS/ETS-mediated morphological change in the development of EFT remain unclarified.

Consistent with the morphological and immunophenotypic changes, the expression pattern of a set of genes in EWS/ETS-expressing UET-13 cells shifted to that in EFT cells (Fig. 7C). Although EWS/ETS expression enhanced the ability of UET-13 cells to invade Matrigel, it did not promote migratory ability and surface-independent growth, as assessed by migration assay and soft agar colony formation assay (data not shown). We also failed to develop EFT-like tumors by injecting EWS/ETS-inducing UET-13 cells into irradiated nude mice treated with tetracycline (data not shown). These results imply that EWS/ETS expression is not sufficient to induce the full transformation in UET-13 cells, and other genetic abnormalities not regulated by EWS/ETS could still be required for the full transformation of human MPCs into EFT cells. An identification of these genes will greatly improve our understanding of the additional genetic lesions that occur after EWS/ETS expression. The genes expressed in EFT cell lines but not in EWS/ETS-expressing UET-13 cells would be candidates for such genes.

In summary, we reported the development of an inducible EWS/ETS expression system in UET-13 cells as a model for the development of EFT in MPCs. In our system, the chimeric genes alone are sufficient to confer EFT-like phenotypes, EFT-specific gene expression pattern, and partial but not full features of malignant transformation. Further analysis using our system should elucidate the pathogenic mechanism by which EFTs develop from MPCs, especially the initiating events mediated by EWS/ETS expression. Our system should also aid in the identification of novel targets of the EWS/ETS-mediated pathway as potential anticancer targets.

ACKNOWLEDGMENTS

This work was supported in part by health and labor sciences research grants (the 3rd-Term Comprehensive 10-Year Strategy for Cancer Control [H19-010], Research on Children and Families [H18-005 and H19-003], Research on Human Genome Tailor Made, and Research on Publicly Essential Drugs and Medical Devices [H18-005]) and a grant for child health and development from the Ministry of Health, Labor and Welfare of Japan, JSPS (Kakenhi 18790263). This work was also supported by a CREST, JST grant from the Japan Health Sciences Foundation for Research on Publicly Essential Drugs and Medical Devices and the Budget for Nuclear Research of the Ministry of Education, Culture, Sports, Science and Technology, based on screening and counseling by the Atomic Energy Commission. Y. Miyagawa is an awardee of a research resident fellowship from the Foundation for Promotion of Cancer Research (Japan) for the 3rd-Term Comprehensive 10-Year Strategy for Cancer Control.

We are grateful to T. Motoyama for the NRS-1 cell line. We respectfully thank S. Yamauchi for her secretarial work and M. Itagaki for many helpful discussions and support.

REFERENCES

1. **Akagi, T.** 2004. Oncogenic transformation of human cells: shortcomings of rodent model systems. Trends Mol. Med. **10**:542–548.
2. **Ambros, I. M., P. F. Ambros, S. Strehl, H. Kovar, H. Gadner, and M. Salzer-Kuntschik.** 1991. MIC2 is a specific marker for Ewing's sarcoma and peripheral primitive neuroectodermal tumors. Evidence for a common histogenesis of Ewing's sarcoma and peripheral primitive neuroectodermal tumors from MIC2 expression and specific chromosome aberration. Cancer **67**:1886–1893.
3. **Arvand, A., and C. T. Denny.** 2001. Biology of EWS/ETS fusions in Ewing's family tumors. Oncogene **20**:5747–5754.
4. **Bertani, N., P. Malatesta, G. Volpi, P. Sonego, and R. Perris.** 2005. Neurogenic potential of human mesenchymal stem cells revisited: analysis by immunostaining, time-lapse video and microarray. J. Cell Sci. **118**:3925–3936.
5. **Bloom, E. T.** 1972. Further definition by cytotoxicity tests of cell surface antigens of human sarcomas in culture. Cancer Res. **32**:960–967.
6. **Castillero-Trejo, Y., S. Eliazer, L. Xiang, J. A. Richardson, and R. L. Ilaria, Jr.** 2005. Expression of the EWS/FLI-1 oncogene in murine primary bone-derived cells results in EWS/FLI-1-dependent, Ewing sarcoma-like tumors. Cancer Res. **65**:8698–8705.
7. **Colter, D. C., I. Sekiya, and D. J. Prockop.** 2001. Identification of a subpopulation of rapidly self-renewing and multipotential adult stem cells in colonies of human marrow stromal cells. Proc. Natl. Acad. Sci. USA **98**: 7841–7845.
8. **Conget, P. A., and J. J. Minguell.** 1999. Phenotypical and functional properties of human bone marrow mesenchymal progenitor cells. J. Cell. Physiol. **181**:67–73.
9. **Davis, S., and P. S. Meltzer.** 2006. Ewing's sarcoma: general insights from a rare model. Cancer Cell **9**:331–332.
10. **Deneen, B., and C. T. Denny.** 2001. Loss of p16 pathways stabilizes EWS/FLI1 expression and complements EWS/FLI1 mediated transformation. Oncogene **20**:6731–6741.
11. **Deneen, B., S. M. Welford, T. Ho, F. Hernandez, I. Kurland, and C. T. Denny.** 2003. PIM3 proto-oncogene kinase is a common transcriptional target of divergent EWS/ETS oncoproteins. Mol. Cell. Biol. **23**:3897–3908.
12. **Eliazer, S., J. Spencer, D. Ye, E. Olson, and R. L. Ilaria, Jr.** 2003. Alteration of mesodermal cell differentiation by EWS/FLI-1, the oncogene implicated in Ewing's sarcoma. Mol. Cell. Biol. **23**:482–492.
13. **Fujii, Y., Y. Nakagawa, T. Hongo, Y. Igarashi, Y. Naito, and M. Maeda.** 1989. Cell line of small round cell tumor originating in the chest wall: W-ES. Hum. Cell **2**:190–191. (In Japanese.)
14. **Fukuma, M., H. Okita, J. Hata, and A. Umezawa.** 2003. Upregulation of Id2, an oncogenic helix-loop-helix protein, is mediated by the chimeric EWS/ets protein in Ewing sarcoma. Oncogene **22**:1–9.
15. **Gilbert, F., G. Balaban, P. Moorhead, D. Bianchi, and H. Schlesinger.** 1982.

Abnormalities of chromosome 1p in human neuroblastoma tumors and cell lines. Cancer Genet. Cytogenet. 7:33–42.
16. **Girish, V., and A. Vijayalakshmi.** 2004. Affordable image analysis using NIH Image/ImageJ. Indian J. Cancer **41**:47.
17. **Gonzalez, I., F. J. Andreu, A. Panizo, S. Inoges, A. Fontalba, J. L. Fernandez-Luna, M. Gaboli, L. Sierrasesumaga, S. Martin-Algarra, J. Pardo, F. Prosper, and E. de Alava.** 2004. Imatinib inhibits proliferation of Ewing tumor cells mediated by the stem cell factor/KIT receptor pathway, and sensitizes cells to vincristine and doxorubicin-induced apoptosis. Clin. Cancer Res. **10**:751–761.
18. **Hansen, M. B., S. E. Nielsen, and K. Berg.** 1989. Re-examination and further development of a precise and rapid dye method for measuring cell growth/cell kill. J. Immunol. Methods **119**:203–210.
19. **Hara, S., E. Ishii, S. Tanaka, J. Yokoyama, K. Katsumata, J. Fujimoto, and J. Hata.** 1989. A monoclonal antibody specifically reactive with Ewing's sarcoma. Br J. Cancer **60**:875–879.
20. **Hatori, M., H. Doi, M. Watanabe, H. Sasano, M. Hosaka, S. Kotajima, F. Urano, J. Hata, and S. Kokubun.** 2006. Establishment and characterization of a clonal human extraskeletal Ewing's sarcoma cell line, EES1. Tohoku J. Exp. Med. **210**:221–230.
21. **Homma, C., Y. Kaneko, K. Sekine, S. Hara, J. Hata, and M. Sakurai.** 1989. Establishment and characterization of a small round cell sarcoma cell line, SCCH-196, with t(11;22)(q24;q12). Jpn. J. Cancer Res. **80**:861–865.
22. **Hubert, R. S., I. Vivanco, E. Chen, S. Rastegar, K. Leong, S. C. Mitchell, R. Madraswala, Y. Zhou, J. Kuo, A. B. Raitano, A. Jakobovits, D. C. Saffran, and D. E. Afar.** 1999. STEAP: a prostate-specific cell-surface antigen highly expressed in human prostate tumors. Proc. Natl. Acad. Sci. USA **96**:14523–14528.
23. **Hu-Lieskovan, S., J. Zhang, L. Wu, H. Shimada, D. E. Schofield, and T. J. Triche.** 2005. EWS-FLI1 fusion protein up-regulates critical genes in neural crest development and is responsible for the observed phenotype of Ewing's family of tumors. Cancer Res. **65**:4633–4644.
24. **Im, Y. H., H. T. Kim, C. Lee, D. Poulin, S. Welford, P. H. Sorensen, C. T. Denny, and S. J. Kim.** 2000. EWS-FLI1, EWS-ERG, and EWS-ETV1 oncoproteins of Ewing tumor family all suppress transcription of transforming growth factor beta type II receptor gene. Cancer Res. **60**:1536–1540.
25. **Jones, E. A., S. E. Kinsey, A. English, R. A. Jones, L. Straszynski, D. M. Meredith, A. F. Markham, A. Jack, P. Emery, and D. McGonagle.** 2002. Isolation and characterization of bone marrow multipotential mesenchymal progenitor cells. Arthritis Rheum. **46**:3349–3360.
26. **Khoury, J. D.** 2005. Ewing sarcoma family of tumors. Adv. Anat. Pathol. **12**:212–220.
27. **Kiyokawa, N., Y. Kokai, K. Ishimoto, H. Fujita, J. Fujimoto, and J. I. Hata.** 1990. Characterization of the common acute lymphoblastic leukaemia antigen (CD10) as an activation molecule on mature human B cells. Clin. Exp. Immunol. **79**:322–327.
28. **Konemann, S., T. Bolling, A. Schuck, J. Malath, A. Kolkmeyer, K. Horn, D. Riesenbeck, S. Hesselmann, R. Diallo, J. Vormoor, and N. A. Willich.** 2003. Effect of radiation on Ewing tumour subpopulations characterized on a single-cell level: intracellular cytokine, immunophenotypic, DNA and apoptotic profile. Int. J. Radiat. Biol. **79**:181–192.
29. **Kovar, H., and A. Bernard.** 2006. CD99-positive "Ewing's sarcoma" from mouse bone marrow-derived mesenchymal progenitor cells? Cancer Res. **66**:9786.
30. **Kovar, H., M. Dworzak, S. Strehl, E. Schnell, I. M. Ambros, P. F. Ambros, and H. Gadner.** 1990. Overexpression of the pseudoautosomal gene MIC2 in Ewing's sarcoma and peripheral primitive neuroectodermal tumor. Oncogene **5**:1067–1070.
31. **Lessnick, S. L., C. S. Dacwag, and T. R. Golub.** 2002. The Ewing's sarcoma oncoprotein EWS/FLI induces a p53-dependent growth arrest in primary human fibroblasts. Cancer Cell **1**:393–401.
32. **Lin, P. P., R. I. Brody, A. C. Hamelin, J. E. Bradner, J. H. Healey, and M. Ladanyi.** 1999. Differential transactivation by alternative EWS-FLI1 fusion proteins correlates with clinical heterogeneity in Ewing's sarcoma. Cancer Res. **59**:1428–1432.
33. **Lipinski, M., K. Braham, I. Philip, J. Wiels, T. Philip, C. Goridis, G. M. Lenoir, and T. Tursz.** 1987. Neuroectoderm-associated antigens on Ewing's sarcoma cell lines. Cancer Res. **47**:183–187.
34. **Lochter, A., A. Srebrow, C. J. Sympson, N. Terracio, Z. Werb, and M. J. Bissell.** 1997. Misregulation of stromelysin-1 expression in mouse mammary tumor cells accompanies acquisition of stromelysin-1-dependent invasive properties. J. Biol. Chem. **272**:5007–5015.
35. **May, W. A., A. Arvand, A. D. Thompson, B. S. Braun, M. Wright, and C. T. Denny.** 1997. EWS/FLI1-induced manic fringe renders NIH 3T3 cells tumorigenic. Nat. Genet. **17**:495–497.
36. **May, W. A., S. L. Lessnick, B. S. Braun, M. Klemsz, B. C. Lewis, L. B. Lunsford, R. Hromas, and C. T. Denny.** 1993. The Ewing's sarcoma EWS/FLI-1 fusion gene encodes a more potent transcriptional activator and is a more powerful transforming gene than FLI-1. Mol. Cell. Biol. **13**:7393–7398.
37. **Miyagawa, Y., J. M. Lee, T. Maeda, K. Koga, Y. Kawaguchi, and T. Kusakabe.** 2005. Differential expression of a Bombyx mori AHA1 homologue during spermatogenesis. Insect Mol. Biol. **14**:245–253.
38. **Mori, T., T. Kiyono, H. Imabayashi, Y. Takeda, K. Tsuchiya, S. Miyoshi, H. Makino, K. Matsumoto, H. Saito, S. Ogawa, M. Sakamoto, J. Hata, and A. Umezawa.** 2005. Combination of hTERT and bmi-1, E6, or E7 induces prolongation of the life span of bone marrow stromal cells from an elderly donor without affecting their neurogenic potential. Mol. Cell. Biol. **25**:5183–5195.
39. **Nishimori, H., Y. Sasaki, K. Yoshida, H. Irifune, H. Zembutso, T. Tanaka, T. Aoyama, T. Hosaka, S. Kawaguchi, T. Wada, J. Hata, J. Toguchida, Y. Nakamura, and T. Tokino.** 2002. The Id2 gene is a novel target of transcriptional activation by EWS-ETS fusion proteins in Ewing family tumors. Oncogene **21**:8302–8309.
40. **Ogose, A., T. Motoyama, T. Hotta, and H. Watanabe.** 1995. In vitro differentiation and proliferation in a newly established human rhabdomyosarcoma cell line. Virchows Arch. **426**:385–391.
41. **Prieur, A., F. Tirode, P. Cohen, and O. Delattre.** 2004. EWS/FLI-1 silencing and gene profiling of Ewing cells reveal downstream oncogenic pathways and a crucial role for repression of insulin-like growth factor binding protein 3. Mol. Cell. Biol. **24**:7275–7283.
42. **Quirici, N., D. Soligo, P. Bossolasco, F. Servida, C. Lumini, and G. L. Deliliers.** 2002. Isolation of bone marrow mesenchymal stem cells by anti-nerve growth factor receptor antibodies. Exp. Hematol. **30**:783–791.
43. **Reyes, M., T. Lund, T. Lenvik, D. Aguiar, L. Koodie, and C. M. Verfaillie.** 2001. Purification and ex vivo expansion of postnatal human marrow mesodermal progenitor cells. Blood **98**:2615–2625.
44. **Reyes, M., and C. M. Verfaillie.** 2001. Characterization of multipotent adult progenitor cells, a subpopulation of mesenchymal stem cells. Ann. N. Y. Acad. Sci. **938**:231–235.
45. **Riggi, N., L. Cironi, P. Provero, M. L. Suva, K. Kaloulis, C. Garcia-Echeverria, F. Hoffmann, A. Trumpp, and I. Stamenkovic.** 2005. Development of Ewing's sarcoma from primary bone marrow-derived mesenchymal progenitor cells. Cancer Res. **65**:11459–11468.
46. **Riggi, N., M. L. Suva, and I. Stamenkovic.** 2006. Ewing's sarcoma-like tumors originate from EWS-FLI-1-expressing mesenchymal progenitor cells. Cancer Res. **66**:9786.
47. **Sekiguchi, M., T. Oota, K. Sakakibara, N. Inui, and G. Fujii.** 1979. Establishment and characterization of a human neuroblastoma cell line in tissue culture. Jpn. J. Exp. Med. **49**:67–83.
48. **Smith, R., L. A. Owen, D. J. Trem, J. S. Wong, J. S. Whangbo, T. R. Golub, and S. L. Lessnick.** 2006. Expression profiling of EWS/FLI identifies NKX2.2 as a critical target gene in Ewing's sarcoma. Cancer Cell **9**:405–416.
49. **Staege, M. S., C. Hutter, I. Neumann, S. Foja, U. E. Hattenhorst, G. Hansen, D. Afar, and S. E. Burdach.** 2004. DNA microarrays reveal relationship of Ewing family tumors to both endothelial and fetal neural crest-derived cells and define novel targets. Cancer Res. **64**:8213–8221.
50. **Takeda, Y., T. Mori, H. Imabayashi, T. Kiyono, S. Gojo, S. Miyoshi, N. Hida, M. Ita, K. Segawa, S. Ogawa, M. Sakamoto, S. Nakamura, and A. Umezawa.** 2004. Can the life span of human marrow stromal cells be prolonged by bmi-1, E6, E7, and/or telomerase without affecting cardiomyogenic differentiation? J. Gene Med. **6**:833–845.
51. **Tondreau, T., N. Meuleman, A. Delforge, M. Dejeneffe, R. Leroy, M. Massy, C. Mortier, D. Bron, and L. Lagneaux.** 2005. Mesenchymal stem cells derived from CD133-positive cells in mobilized peripheral blood and cord blood: proliferation, Oct4 expression, and plasticity. Stem Cells **23**:1105–1112.
52. **Torchia, E. C., S. Jaishankar, and S. J. Baker.** 2003. Ewing tumor fusion proteins block the differentiation of pluripotent marrow stromal cells. Cancer Res. **63**:3464–3468.
53. **Woodbury, D., E. J. Schwarz, D. J. Prockop, and I. B. Black.** 2000. Adult rat and human bone marrow stromal cells differentiate into neurons. J. Neurosci. Res. **61**:364–370.

MOLECULAR AND CELLULAR BIOLOGY, June 2008, p. 3882
0270-7306/08/$08.00+0 doi:10.1128/MCB.00557-08

Vol. 28, No. 11

ERRATUM

Inducible Expression of Chimeric EWS/ETS Proteins Confers Ewing's Family Tumor-Like Phenotypes to Human Mesenchymal Progenitor Cells

Yoshitaka Miyagawa, Hajime Okita, Hideki Nakaijima, Yasuomi Horiuchi, Ban Sato, Tomoko Taguchi, Masashi Toyoda, Yohko U. Katagiri, Junichiro Fujimoto, Jun-ichi Hata, Akihiro Umezawa, and Nobutaka Kiyokawa

Department of Developmental Biology, National Research Institute for Child Health and Development, 2-10-1, Okura, Setagaya-ku, Tokyo 157-8535, Japan; National Research Institute for Child Health and Development, 2-10-1, Okura, Setagaya-ku, Tokyo 157-8535, Japan; and Department of Reproductive Biology, National Research Institute for Child Health and Development, 2-10-1, Okura, Setagaya-ku, Tokyo 157-8535, Japan

Volume 28, no. 7, p. 2125–2137, 2008. Page 2131: The boxheads for Table 2 should appear as shown below.

MPC status[a]	CD marker	Result for[b]: UET-13	UET-13R		UET-13TR-EWS/FLI		UET-13TR-EWS/ERG		RD-ES	SK-ES1	EFT status[c]
			Tet$^-$	Tet$^+$	Tet$^-$	Tet$^+$	Tet$^-$	Tet$^+$			

Int J Hematol (2008) 87:75–77
DOI 10.1007/s12185-007-0007-x

CASE REPORT

Evans syndrome in a patient with Langerhans cell histiocytosis: possible pathogenesis of autoimmunity in LCH

Yoichiro Tsuji · Kazuhiro Kogawa · Kohsuke Imai · Hirokazu Kanegane · Junichiro Fujimoto · Shigeaki Nonoyama

Received: 11 June 2007 / Revised: 25 September 2007 / Accepted: 9 October 2007 / Published online: 27 November 2007

Abstract We report a 1-year-old girl with Evans syndrome coexisting with histologically confirmed Langerhans cell histiocytosis (LCH) affecting the cervical lymph nodes, liver, and spleen. Anti-cardiolipin antibody, anti-SS-A antibody, and anti-SS-B antibody as well as a direct antiglobulin test and platelet-associated IgG were all positive at the onset, and these autoantibodies became negative with the resolution of LCH by chemotherapy. Serum T-helper-2 (Th2) cytokine levels such as those of interleukin (IL)-6 and IL-10 were high whereas those of Th1 cytokines such as IL-2 and interferon-gamma were low at the onset, and this cytokine imbalance was normalized during the resolution of LCH. These results suggest that cytokine imbalance due to LCH led to multiple autoimmune phenomena in the present patient.

Keywords Langerhans cell histiocytosis · Evans syndrome · Cytokines · Hemolytic anemia · ITP · Autoimmune

Y. Tsuji (✉) · K. Kogawa · K. Imai · S. Nonoyama
Department of Pediatrics, National Defense Medical College, 3-2 Namiki, Tokorozawa, Saitama 359-0042, Japan
e-mail: ytsuji@ndmc.ac.jp

H. Kanegane
Department of Pediatrics, Faculty of Medicine, University of Toyama, Toyama, Japan

J. Fujimoto
Division of Developmental Biology and Pathology, National Research Institute for Child Health and Development, Tokyo, Japan

1 Introduction

Langerhans cell histiocytosis (LCH) is a rare neoplastic disease with a wide clinical spectrum, ranging from a spontaneously regressing solitary lesion of bone to a multisystem, life-threatening disorder [1, 2]. The association of LCH with autoimmune disease is extremely rare, and its coexistence with Evans syndrome has not been reported to date.

Herein, we report a patient with LCH coexisting with autoimmune phenomena including Evans syndrome, and discuss a possible pathogenesis of these rare phenomena.

2 Case report

A 1-year-old female patient was referred to our hospital because of prolonged fever, enlarged cervical lymph nodes, and hepatosplenomegaly. On admission, the bilateral cervical lymph nodes were palpable over a region 10 cm in diameter, and the liver and spleen were palpable 11 and 5 cm below the costal margin, respectively. The white blood cell count was 15.4×10^9/L with 28% bands, 68% segments, 3% lymphocytes, and 1% monocytes. Hemoglobin, the reticulocyte count, and platelet count were 4.4 g/dL, 145×10^9/L, and 48×10^9/L, respectively. Serum LDH was high (473 IU/L), haptoglobin was low (2.4 mg/L), and total bilirubin was normal (0.8 mg/dL). Coagulation studies revealed an international normalized ratio of 1.57 and activated partial thromboplastin time of 49.5 s. Serum IgG was high (1,610 mg/dL). Bone marrow aspiration revealed a normal nuclear cell count (260×10^6/mL), increased megakaryocyte count (9×10^4/mL) and no proliferation of LCH cells. A direct antiglobulin test (IgG and C3) (DAT) was positive and

platelet-associated IgG (PA-IgG) was high (175.2 ng/10^7 cells, normal value <25). Thus, she was diagnosed with Evans syndrome. In addition, anti-cardiolipin Ab, anti-SS-A Ab, and anti-SS-B Ab were all positive at the disease onset (Table 1). Analysis of lymphocyte subsets revealed marked B cell proliferation (60% of total lymphocytes). As autoimmune lymphoproliferative syndrome (ALPS) was suspected [3], we investigated Fas-mediated apoptosis and TCR$\alpha\beta$+CD4-CD8- T cells (double-negative T cells: DNT). However, Fas-mediated apoptosis was normal and DNT cells did not increase in number (data not shown). As shown in Fig. 1, biopsy of the cervical lymph nodes revealed that S100 protein was positive, Langerin-positive, and CD1a-positive atypical cells were abundant in the specimen, and so the diagnosis of LCH was confirmed. Involved organs were the cervical lymph nodes, liver, and spleen, without any characteristic bone lesion. Several serum cytokines were longitudinally investigated via enzyme immunoassay (Table 1). T-helper-2 (Th2) cytokine levels such as those of interleukin (IL)-6 and IL-10 were high whereas those of Th1 cytokines such as IL-2 and interferon gamma (IFN-γ) were low at the onset.

The patient was treated with induction chemotherapy according to the JLSG-02 protocol, which is almost identical to the JLSG-96 protocol with only minor modification [4], consisting of prednisolone, cytosine arabinoside, and vincristine. Complete remission (CR) was achieved with the resolution of anemia and thrombocytopenia, and all autoantibodies became negative within a few weeks after the beginning of chemotherapy. The normalization of high levels of Th2 cytokines was observed with the resolution of the disease (Table 1). The patient completed maintenance chemotherapy about 1 year ago and remains in CR without treatment.

3 Discussion

LCH with autoimmune disease is rare, but coexisting organ-specific autoimmune disorders such as myasthenia gravis [5] and membranous nephropathy [6] with LCH have been reported in the past. Systemic autoimmune disorder has been reported in only one patient, who had LCH with systemic lupus erythematosus [7]. Hematologic autoimmune disorder has been reported in only one LCH patient with AIHA [8]. Recently, it has been suggested that central diabetes insipidus in LCH, a major complication of this disorder, is caused by vasopressin-cell autoantibody [9]. Thus autoimmunity in LCH may be more common than has been expected. Although Evans syndrome with other autoimmune disorders has been reported in the past [10], coexistence with LCH in this syndrome has not been reported to date. As multiple autoantibodies including DAT and PA-IgG were positive, Evans syndrome was strongly suspected in our LCH patient.

It is well-known that hypercytokinemia plays a central role in the pathogenesis of LCH [11]. In our patient, serum Th2 cytokine levels such as those of IL-6 and IL-10 were high whereas those of Th1 cytokines such as IL-2 and IFN-γ were low at diagnosis, and this cytokine imbalance was normalized with the resolution of LCH. Multiple autoantibodies were initially positive at diagnosis and disappeared

Table 1 Serum autoantibodies, cytokines, and lymphocyte subsets of the patient

	On admission	6th week (at the end of induction)	14th week (during maintenance)	53rd week (at the end of maintenance)	69th week (recent)
DAT	Positive	Negative	Negative	Negative	Negative
PA-IgG (<25)	175.2	18.7		14.1	
ACLAb (<10)	15	<8	<8	<8	12
SS-A Ab (<10.0)	38.8	7.1	<5.0	<5.0	<5.0
SSB Ab (15.0)	15.3	5	<5.0	<5.0	<5.0
IFN-γ (<0.1)	0.2			<0.1	
IL-2 (<0.8)	<0.8			<0.8	
IL-6 (4.0)	180	1.5	0.5	0.3	2.1
IL-10 (<5.0)	86	<2	<2	<2	<2
CD3 (+) cells (%)	34.7	64.1		60.4	
CD4 (+) cells (%)	24	30.8		32.5	
CD8 (+) cells (%)	8.5	30.7		23.3	
CD19 (+) cells (%)	60.7	25.7		33.5	

Numbers of parentheses in the left column represent normal values

DAT direct antiglobulin test, *PA-IgG* platelet-associated IgG, *ACLAb* anti-phospholipid antibody, *SS-A Ab* anti-SS-A antibody, *SS-B Ab* anti-SS-B antibody, *IFN-γ* interferon gamma, *IL* interleukin

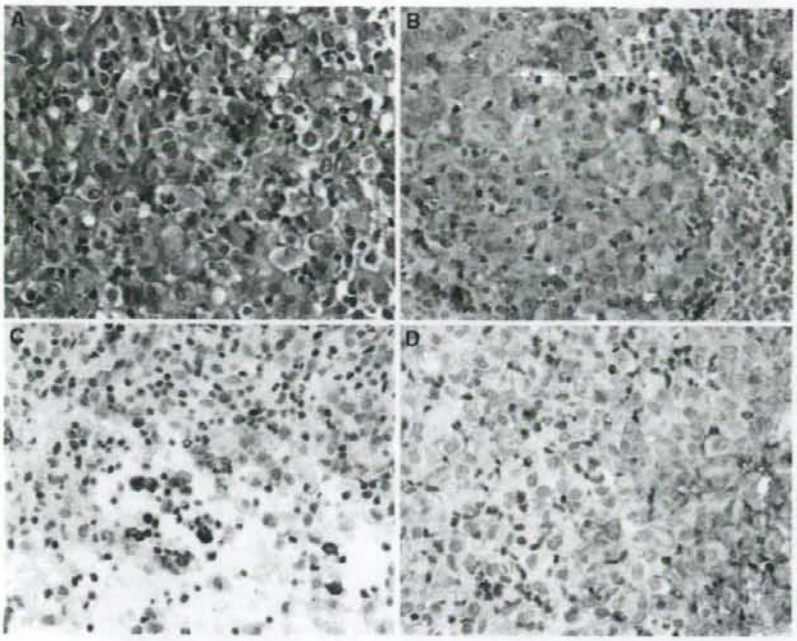

Fig. 1 Biopsy specimen of a cervical lymph node. Atypical, large Langerhans cells are abundant (**a**, hematoxylin-eosin). Immunohistochemical stains revealed that these cells were positive for S-100 (**b**), Langerin (**c**), and CD 1a (**d**)

soon after treatment. These results suggest that the cytokine imbalance had led to the production of multiple autoantibodies in our patient [12].

In summary, cytokine imbalance may have played an important role in the pathogenesis of autoimmunity in our LCH patient. Further investigation is warranted to resolve the pathogenesis of this rare, or may be more common than has been expected, complication in LCH.

Acknowledgments This report was supported by a grant from Kawano Masanori Memorial Foundation for Promotion of Pediatrics.

References

1. Egeler RM, D'Angio GJ. Langerhans cell histiocytosis. J Pediatr. 1995;127(1):1–11.
2. Arico M, Egeler RM. Clinical aspects of Langerhans cell histiocytosis. Hematol Oncol Clin North Am. 1998;12(2):247–58.
3. Teachey DT, Manno CS, Axsom KM, et al. Unmasking Evans syndrome: T-cell phenotype and apoptotic response reveal autoimmune lymphoproliferative syndrome (ALPS). Blood. 2005;105(6):2443–8.
4. Morimoto A, Ikushima S, Kinugawa N, et al. Improved outcome in the treatment of pediatric multifocal Langerhans cell histiocytosis: results from the Japan Langerhans Cell Histiocytosis Study Group-96 protocol study. Cancer. 2006;107(3):613–9.
5. Gilcrease MZ, Rajan B, Ostrowski ML, et al. Localized thymic Langerhans' cell histiocytosis and its relationship with myasthenia gravis. Immunohistochemical, ultrastructural, and cytometric studies. Arch Pathol Lab Med. 1997;121(2):134–8.
6. Rachima CM, Cohen E, Iaina NL, et al. A case of Langerhans'-cell histiocytosis with membranous nephropathy. Am J Kidney Dis. 2004;43(2):e3–9.
7. Robak T, Kordek R, Robak E, et al. Langerhans cell histiocytosis in a patient with systemic lupus erythematosus: a clonal disease responding to treatment with cladribine, and cyclophosphamide. Leuk Lymphoma. 2002;43(10):2041–6.
8. Oliveira MC, Oliveira BM, Murao M, et al. Clinical course of autoimmune hemolytic anemia: an observational study. J Pediatr (Rio J). 2006;82(1):58–62.
9. Maghnie M, Ghirardello S, De Bellis A, et al. Idiopathic central diabetes insipidus in children and young adults is commonly associated with vasopressin-cell antibodies and markers of autoimmunity. Clin Endocrinol (Oxf). 2006;65(4):470–8.
10. Savasan S, Warrier I, Ravindranath Y. The spectrum of Evans' syndrome. Arch Dis Child. 1997;77(3):245–8.
11. Egeler RM, Favara BE, van Meurs M, et al. Differential In situ cytokine profiles of Langerhans-like cells and T cells in Langerhans cell histiocytosis: abundant expression of cytokines relevant to disease and treatment. Blood. 1999;94(12):4195–201.
12. Barcellini W, Clerici G, Montesano R, et al. In vitro quantification of anti-red blood cell antibody production in idiopathic autoimmune haemolytic anaemia: effect of mitogen and cytokine stimulation. Br J Haematol. 2000;111(2):452–60.

CD43, but not P-Selectin Glycoprotein Ligand-1, Functions as an E-Selectin Counter-Receptor in Human Pre-B–Cell Leukemia NALL-1

Chizu Nonomura,[1,3] Jiro Kikuchi,[1] Nobutaka Kiyokawa,[4] Hidenori Ozaki,[1] Kanae Mitsunaga,[1] Hidenobu Ando,[1] Akiko Kanamori,[5] Reiji Kannagi,[5] Junichiro Fujimoto,[4] Kazuo Muroi,[6] Yusuke Furukawa,[7] and Mitsuru Nakamura[1,2,3]

[1]Cell Regulation Analysis Team, Research Center for Medical Glycoscience, National Institute of Advanced Industrial Science and Technology; [2]Function of Biomolecule, University of Tsukuba, Tsukuba, Japan; [3]Core Research for Evolution Science and Technology of Japan Science and Technology Agency, Kawaguchi, Japan; [4]Department of Developmental Biology, National Research Institute of Child Health and Development, Tokyo, Japan; [5]The Department of Molecular Pathology, Aichi Cancer Center, Chikusa-ku, Nagoya, Japan; and [6]Division of Cell Transplantation and Transfusion and [7]Division of Stem Cell Regulation, Jichi Medical School, Shimotsuke, Tochigi, Japan

Abstract

B-cell precursor acute lymphoblastic leukemia (BCP-ALL/B-precursor ALL) is characterized by a high rate of tissue infiltration. The mechanism of BCP-ALL cell extravasation is not fully understood. In the present study, we have investigated the major carrier of carbohydrate selectin ligands in the BCP-ALL cell line NALL-1 and its possible role in the extravascular infiltration of the leukemic cells. B-precursor ALL cell lines and clinical samples from patients with BCP-ALL essentially exhibited positive flow cytometric reactivity with E-selectin, and the reactivity was significantly diminished by *O*-sialoglycoprotein endopeptidase treatment in NALL-1 cells. B-precursor ALL cell lines adhered well to E-selectin but only very weakly to P-selectin with low-shear-force cell adhesion assay. Although BCP-ALL cell lines did not express the well-known core protein P-selectin glycoprotein ligand-1 (PSGL-1), a major proportion of the carbohydrate selectin ligand was carried by a sialomucin, CD43, in NALL-1 cells. Most clinical samples from patients with BCP-ALL exhibited a PSGL-1$^{neg/low}$/CD43^{high} phenotype. NALL-1 cells rolled well on E-selectin, but knockdown of CD43 on NALL-1 cells resulted in reduced rolling activity on E-selectin. In addition, the CD43 knockdown NALL-1 cells showed decreased tissue engraftment compared with the control cells when introduced into γ-irradiated immunodeficient mice. These results strongly suggest that CD43 but not PSGL-1 plays an important role in the extravascular infiltration of NALL-1 cells and that the degree of tissue engraftment of B-precursor ALL cells may be controlled by manipulating CD43 expression. [Cancer Res 2008;68(3):790–9]

Introduction

Infiltrating ability is one of the most important characteristics of leukemia cells (1, 2). After infiltration and engraftment, a proportion of leukemia cells is thought to be maintained in microenvironmental niches and escape the effects of anticancer drugs (3, 4). A small population of leukemia cells is known for their ability to transplant disease to a recipient and is experimentally called leukemic stem cells (3). They also home, engraft, and are maintained in their supportive microenvironmental niches (3, 5–7). Therefore, inhibition of leukemia cell infiltration and engraftment may improve the treatment outcome of patients with leukemia.

B-cell precursor acute lymphoblastic leukemia (BCP-ALL/B-precursor ALL) is the most common childhood malignancy and the second most common acute leukemia in adults (2). Eighty percent and 76% of ALLs are of B-lineage in childhood and adulthood, respectively, 95% of B-lineage acute leukemias are BCP-ALLs in adulthood, and B-precursor ALL consists of pro-B ALL, common ALL, and pre-B ALL (2). Although the remission rate is relatively high in patients with BCP-ALL, the disease often relapses in the central nervous system (CNS) and peripheral organs (2). This is in part attributable to the ability of BCP-ALL cells to infiltrate and engraft into the liver, spleen, and CNS. Hepatomegaly, splenomegaly, and lymphadenopathy are found in about 69% to 86% of patients at the first medical examination and hepatosplenomegaly per se is one of the risk factors (1, 8). Infiltration to the CNS is found in <10% of patient at the first examination but such patients are also in a high-risk group (1). In this context, manipulating the tissue infiltration of BCP-ALL cells could be important.

Leukocytes emigrate from blood into peripheral tissues through the sequential interactions of selectins with their ligands, chemokines with their receptors, and integrins with their ligands (9–11). Precursor-B cells and BCP-ALL cell lines are known to express selectin ligands, chemokine receptors, and integrins, and these adhesion molecules may play important roles in cell migration. Carbohydrate selectin ligands are expressed in BCP leukemia cells and the down-regulation of their expression influences tissue infiltration (12). CXCR4, a receptor for stromal cell-derived factor-1, is involved in the localization of BCP-ALL cells and precursor-B cells within the bone marrow (BM) stromal layer (13, 14). β_1/β_2 integrins are expressed in BCP-ALL cells (15) and involved in the intercellular association between BCP-ALL cells and BM stromas (16). Thus, it is important to reveal which adhesion molecules are expressed and how their expression is regulated to understand the mechanisms of leukemia cell homing and engraftment.

We reported previously that BCP-ALL cell lines express a sialyl-Lewis-X (sLe^X)-related carbohydrate structure, the amount of

Requests for reprints: Mitsuru Nakamura, Cell Regulation Analysis Team, Research Center for Medical Glycoscience, National Institute of Advanced Industrial Science and Technology, Central-2, 1-1-1 Umezono, Tsukuba 305-8568, Japan. Phone: 81-29-861-2745; Fax: 81-29-861-2744; E-mail: owl.nakamura@aist.go.jp.

doi:10.1158/0008-5472.CAN-07-1459

which is regulated by core 2 β1,6-*N*-acetylglucosaminyltransferase-1 (C2GnT1) during differentiation (17–19). Another important glycosyltransferase, α1,3-fucosyltransferase-VII, was involved in sLe^X biosynthesis in BCP-ALL cells but did not exhibit significant change during pre-B-cell differentiation (17, 18). Knockdown of C2GnT1 in a B-precursor ALL cell line resulted in a reduction in leukemic cell tissue migration using mouse model (12). Moreover, the sLe^X-related structure was mainly located on an *O*-glycosylated protein (17, 18). On treatment of BCP-ALL cells with an *O*-sialoglycoprotein–specific endopeptidase, leukemic cell migration reduced *in vivo* (12).

For the selectin counter-receptor in leukocytes, P-selectin glycoprotein ligand-1 (PSGL-1) has been identified as the major ligand of P-selectin and E-selectin (20–22). As for BCP-ALL cells, the major carrier of selectin ligands is expected to be a sialomucin (12, 17, 18) but has yet to be identified. In the present study, we show that CD43 functions as an E-selectin counter-receptor in a BCP-ALL cell line. BCP-ALL cells exhibited a $PSGL\text{-}1^{neg/low}$/$CD43^{high}$ phenotype. Although BCP leukemia NALL-1 cells rolled well on E-selectin, knockdown of CD43 resulted in the inhibition of this rolling. In addition, CD43 knockdown led to decreased tissue engraftment in a mouse model. These results suggest that CD43 but not PSGL-1 is a selectin counter-receptor in BCP leukemia NALL-1 cells and plays an important role in their peripheral tissue infiltration and that manipulation of CD43 expression may control the tissue infiltration and engraftment of leukemic cells.

Materials and Methods

Cells and cell culture. The human BCP-ALL cell lines NALL-1, Nalm-6, Nalm-16, Nalm-20, KOPN-8, KOPN-K, BV-173, and LAZ221, the human Burkitt's lymphoma cell line Raji, and the human promyelocytic leukemia cell line HL60 were maintained in RPMI 1640 (Sigma-Aldrich). 293FT cells (Invitrogen) were cultured in DMEM. Chinese hamster ovary (CHO) cells overexpressing human E-selectin (CHO-E cells) were maintained in α-MEM. Cells were cultured at 37°C in 5% CO_2, and the culture medium was supplemented with 10% fetal bovine serum (FBS), 100 units/mL penicillin, and 100 μg/mL streptomycin. BM cells from patients with BCP-ALL were obtained after informed consent and used according to procedures approved by our Institutional Review Boards.

Flow cytometry and cell sorting. Flow cytometry and cell sorting were carried out using FACSAria (BD Biosciences). E-selectin/P-selectin binding was detected using recombinant E-selectin and P-selectin–human immunoglobulin chimeras (E-selectin/Ig and P-selectin/Ig; R&D Systems) in the presence of 1 mmol/L $CaCl_2$ or 10 mmol/L EDTA. R-phycoerythrin (R-PE)–conjugated anti-human Ig (Jackson ImmunoResearch Laboratories) was used as the secondary antibody. The expression of cell surface sialomucins was detected with FITC-conjugated anti-human CD43 (1G10; BD Biosciences), R-PE–conjugated anti-human CD43 (DF-T1; Serotec), or R-PE–conjugated anti-human PSGL-1 antibody (KPL-1; BD Biosciences). The expression of other cell surface molecules was examined using monoclonal antibodies (mAb) for integrin β_1 (CD28; DF5; Chemicon International), VLA4α (CD49d; SG/73; Seikagaku), integrin β_2 (CD18; 6.7; BD Biosciences), LFA1α (CD11a; B-B15; T Cell Diagnostics), ICAM-1 (CD54; VF27; T Cell Diagnostics), L-selectin (CD62L; MHL1; Seikagaku), and CD44 (A3D8; Sigma-Aldrich). The detection was carried out using an indirect immunofluorescence method with secondary anti-mouse Ig antibody conjugated with R-PE. The expression of chemokine receptors was detected with R-PE–conjugated mAbs for CCR7 and CXCR5 (for spleen; R&D Systems), CCR6 and CXCR3 (for liver; R&D Systems), and CXCR4 (12G5 for BM; BD Biosciences).

Low-shear-force cell adhesion assay. This assay was carried out essentially as described (23), except for the cell-labeling procedure. Briefly, multiplate wells were coated with E-selectin/P-selectin/Ig or control IgG at a final concentration of 5 μg/mL overnight at 4°C and washed thrice with PBS. Cells were labeled with 2′,7′-bis-(2-carboxyethyl)-5-(and-6)-carboxyfluorescein, acetoxymethyl ester (BCECF-AM; Molecular Probes), washed with PBS thrice, added to wells coated with selectin/Ig, and incubated for 30 min at 37°C on a shaking incubator at 60 rpm to maintain shear stress conditions. Nonadherent cells were washed off thrice with TBS-$CaCl_2$ or TBS-EDTA. The adherent cells were lysed in 0.5% NP40, and fluorescence intensity was measured with an Arvo SX 1420 multilabel counter (Wallac). The number of cells was calculated from the fluorescence intensity based on a standard curve prepared simultaneously using BCECF-AM–labeled NALL-1 cells.

Inhibition of *O*-glycan biosynthesis and enzymatic breakdown of sialomucins. For the enzymatic breakdown of cell surface sialomucins, cells were cultured for 3 days with daily additions of fresh *O*-sialoglycoprotein endopeptidase (OSGPEPase; Cederlane). The sensitivity of the major selectin ligand carrier protein to OSGPEPase was also examined by treating cell lysates with the endopeptidase for 3 h at 37°C.

Western and selectin blot analyses. Western blotting was performed as described (18) using mAbs for sLe^X (CSLEX1; HB85800; American Type Culture Collection), CD43 [DF-T1 (Sigma-Aldrich) and MEM59 (Monosan)], PSGL-1 (KPL-1), or β-actin (AC-15; Abcam plc). Cell lysates were subjected to a 5.0% or 7.5% SDS-PAGE under reducing or nonreducing conditions and transferred to polyvinylidene difluoride membranes (Bio-Rad Laboratories). After blocking, the membranes were incubated with the primary antibody overnight at 4°C. The blots were incubated with a secondary goat anti-mouse IgM or IgG antibody conjugated with horseradish peroxidase (HRP) for 2 h at room temperature. Signals were visualized with a chemiluminescent substrate (GE Healthcare Bioscience). Selectin blotting was performed essentially as above using E-selectin/Ig, biotin-conjugated anti-human Ig, and HRP-conjugated streptavidin.

Immunoprecipitation. Total cell lysate was precleared using protein L-Sepharose (Pierce Biotechnology) or protein G-Sepharose (Sigma-Aldrich) at 4°C with 1 h of agitation. For each immunoprecipitation reaction, 400 μL of cleared lysate were incubated with 50 μL of CSLEX1 or MEM59 at 4°C overnight, and then 50 μL of protein L-Sepharose or protein G-Sepharose were added and incubated for an additional 1 h. Immunocomplexes were precipitated by centrifugation, washed thrice with radioimmunoprecipitation assay (RIPA) buffer [25 mmol/L Tris-HCl (pH 8.0), 150 mmol/L NaCl, 1% NP40, protease inhibitor mixture (Complete Mini EDTA-free, Roche Diagnostics)], and finally resuspended in the sample buffer and boiled for 5 min. The released proteins were examined by Western blotting.

Biotinylation of cell surface proteins and selectin pull-down. Surface proteins were labeled with biotin using a Sulfo-NHS-LC-Biotin kit according to the manufacturer's instructions (Pierce Biotechnology). Cells were washed thrice with PBS containing 100 mmol/L glycine and lysed with RIPA buffer containing 1 mmol/L $CaCl_2$. The lysate was cleared by centrifugation and the supernatant was pretreated with protein G-Sepharose. After centrifugation, the supernatant was incubated overnight at 4°C with recombinant human E-selectin/Ig and then for another 2 h at 4°C with protein G-Sepharose. After centrifugation, the pellets were directly analyzed by SDS-PAGE or resuspended in immunoprecipitation buffer containing 10 mmol/L EDTA, and the eluted proteins were immunoprecipitated with anti-CD43 and protein G-Sepharose followed by SDS-PAGE. Biotinylated proteins were visualized using streptavidin-HRP and chemiluminescence substrate (GE Healthcare Bioscience).

Gene silencing by lentiviral RNA interference. Short hairpin/short interfering RNA (shRNA/siRNA; refs. 12, 24) was introduced into NALL-1 cells to down-regulate *CD43* expression by the shRNA lentivirus system. Oligonucleotides were chemically synthesized, annealed, terminally phosphorylated, and inserted into the vector pLL3.7. The oligonucleotides containing siRNA target sequences were 5′-tgatgtacaccacttcaataacgcttcctgtcacgttattgaagtggtgtacatcttttttc-3′ (forward #1), 5′-tcgagaaaaaagatgtacaccacttcaataacgtgacaggaagcgttattgaagtggtgtacatca-3′ (reverse #1), 5′-tgagcctttggtctctactattcaagagatagtagagaccaaaggctcttttttc-3′ (forward #2), and 5′-tcgagaaaaaagagcctttggtctctactatctcttgaatagtagagaccaaaggctca-3′ (reverse #2) and those containing a scrambled control sequence of #1 were 5′-tgcaatattacatatacgccttcaagagaggcgtatatgtaatattgcttttttc-3′ (forward) and

5′-tcgagaaaaaagcaatattacatatacgcctctcttgaaggcgtatatgtaatattgca-3′ (reverse); nucleotide sequences corresponding to the siRNA are underlined. The resulting plasmids or the parental pLL3.7, along with lentiviral packaging mix (ViraPower, Invitrogen), were transfected into 293FT cells (Invitrogen) to produce recombinant lentivirus, and the NALL-1 cells were infected with the virus. Enhanced green fluorescent protein–positive cells were purified by FACSAria as shRNA-transfected cell populations (NALL-1siCD43#1, NALL-1siCD43#2, NALL-1scrambled, and NALL-1pLL3.7, respectively).

Gene expression analysis. *CD43* and *β-actin* transcripts were detected by the real-time PCR method. The primer set and probe for *CD43* were as follows: forward, 5′-cacttcaataacaagtgaccctaagg-3′; reverse, 5′-tggtaggttgttggctcaggta-3′; probe, 5′-FAM-ccagacctcagcctacctccctcaa-TAMRA-3′. Those for *matrix metalloproteinase 2* (*MMP2*), *MMP9*, and *β-actin* were purchased from Applied Biosystems. PCR products were continuously measured with a Prism 7000 (Applied Biosystems).

Rolling assay. The rolling assay was performed using a flow chamber (GlycoTech) and CHO-E cells as described (25, 26) with a slight modification. The cells were grown on fibronectin-coated dishes and served as a rolling substrate. The flow chamber for rolling assays was mounted on the stage of an inverted microscope (model IX71, Olympus Products). Test cells were introduced into the flow chamber at a concentration of 5×10^5/mL in RPMI 1640 supplemented with 10% FBS and 1 mmol/L $CaCl_2$. Shear stress in the flow chamber was controlled using a syringe pump (Harvard Apparatus). The number of rolling cells and rolling velocity was measured by tracking an individual cell frame by frame (Digimo).

Migration of BCP-ALL cells *in vivo* model. Test cells, NALL-1siCD43#1 or NALL-1scrambled, were labeled with tetramethylrhodamine-5-isothicyanate (TRITC; Molecular Probes) and control NALL-1 parental cells were labeled with carboxyfluorescein diacetate succinimidyl ester (CFSE; Molecular Probes; ref. 27). Both cells were mixed (1:1) and i.v. injected (1×10^8/mouse) into sublethally γ-irradiated (3.3 Gy) nonobese diabetic/severe combined immunodeficient (NOD/SCID) mice (28). Mice were killed 6 and 24 h after injection, and the spleen, liver, and peripheral blood were sampled. The tissues were minced and filtrated to obtain single-cell suspensions. A BM cell suspension was also prepared from a pair of femurs and tibiae. TRITC-labeled test cells were counted as the engrafted cells in the peripheral organs. The number of test cells injected was normalized using CFSE-labeled control cells at each point of assay. All animal experiments were carried out with approval from our Institutional Review Boards.

Assay for gelatinase activity. Gelatin zymography was used to detect gelatinase activity as described elsewhere (29).

Statistical analysis. The significance of differences between the control and experimental groups was determined with Student's *t* test.

Results

Human BCP-ALL cell lines express selectin ligands. NALL-1 was first reported as a "null" cell line (30) but proved to have B-precursor cell markers (31). The cells are thought to inherit the typical characteristics of common ALL, the major population of BCP-ALLs [terminal deoxynucleotidyl transferase positive (TdT^+)/$CD19^+$/$CD10^+$/sIg^-; ref. 2]. So we chose NALL-1 in this study as a model of BCP-ALL. We first carried out flow cytometry using E-selectin/Ig and P-selectin/Ig to test whether the cells express selectin ligands. As shown in Fig. 1*A* (*top*), NALL-1 cells were positively stained with E-selectin/P-selectin in the presence of $CaCl_2$. Other TdT^+/$CD19^+$/$CD10^+$/sIg^- BCP-ALL cell lines, Nalm-6, Nalm-16, Nalm-20, KOPN-8, KOPN-K, BV-173, and LAZ221, were also essentially positive for E-selectin and/or P-selectin (Table 1A, left two columns). These results suggest that BCP-ALL cells express selectin ligands.

Clinical BCP-ALL samples express selectin ligand. To investigate whether BCP-ALL cell lines inherit the immunophenotype of primary B-precursor ALL cells, we performed a flow cytometric analysis of BM-derived leukemia cells from 13 patients with BCP-ALL. The cells were stained with E-selectin/P-selectin (Table 1B, left two columns). This suggests that BCP-ALL cell lines inherit the immunophenotype of primary B-precursor ALL cells as far as the expression of selectin ligands is concerned.

BCP-ALL cell lines functionally adhere to E-selectin but only very weakly to P-selectin. Although NALL-1 cells bound to both E-selectin/P-selectin in the flow cytometric analysis, it is not clear whether the binding is actually functional. To evaluate the function of selectin ligands on NALL-1 cells, we carried out a low-shear-force cell adhesion assay. The data clearly showed that NALL-1 cells functionally adhere to E-selectin but adhere very poorly to P-selectin (Fig. 1*B*, *white columns*). HL60 cells adhered to both selectins (*gray columns*). The other BCP-ALL cell lines, Nalm-6, Nalm-16, Nalm-20, KOPN-8, KOPN-K, BV-173, and LAZ221, were also tested for functional reactivity with E-selectin/P-selectin. These cells also showed a preference for E-selectin (Fig. 1*C*). The results suggest that the data from flow cytometric analyses should be carefully interpreted and that E-selectin rather than P-selectin is the functional partner of BCP-ALL cell lines.

Identification of the major selectin ligand carrier protein as a sialomucin. Our previous findings suggest that carbohydrate selectin ligands on BCP-ALL cell lines are mainly carried by an *O*-glycosylated protein and that the contribution of *N*-glycans or glycosphingolipids may not be significant (12, 17–19). To test whether the selectin ligand on NALL-1 cells was sensitive to sialomucin-specific endopeptidase, flow cytometry was first carried out using NALL-1 cells treated with OSGPEP'ase for 3 days. As exhibited in Fig. 1*A* (*bottom left*), the reactivity with E-selectin decreased significantly. This suggests that the E-selectin ligand on NALL-1 cells is carried by sialomucin(s). On the other hand, the effect of OSGPEP'ase on P-selectin reactivity was minimal (*bottom right*). This suggests that the P-selectin ligand on NALL-1 cells is carried by some OSGPEP'ase-resistant glycoconjugate(s) or the reactivity with P-selectin detected by flow cytometry is not functional in NALL-1 cells. In the subsequent analyses of this study, we focused on the identification and function(s) of the OSGPEP'ase-sensitive E-selectin ligand on BCP-ALL cells.

Subsequently, we performed an immunoblot analysis of NALL-1 cell lysate to detect the E-selectin counter-receptor(s). As shown in Fig. 1*D* (*lane 1*), we observed one major sLe^X-carrying protein. This major sLe^X carrier had an apparent molecular mass of ~135 kDa on 7.5% SDS-PAGE (*lane 5*) and was designated gp135. To identify gp135 as a sialomucin, cell lysates were treated with OSGPEP'ase and analyzed using immunoblotting with anti-sLe^X mAb. As shown in *lane 2*, gp135 was OSGPEP'ase sensitive; the signal became faint after the treatment. As a positive control for the enzyme treatment, the blot was reprobed with an anti-CD43 mAb, DF-T1. CD43 was sensitive to OSGPEP'ase (*lane 4*). To our surprise, CD43 was identical or very similar in size to gp135 (*lanes 1* and *3*). To test whether gp135 was an E-selectin ligand carrier, we performed blotting of NALL-1 cell lysate. With the blotting, a main band (~135 kDa) was detected along with a minor signal (~180 kDa; *lane 7*). The intensity of the major gp135 signal was reduced on pretreatment with OSGPEP'ase, whereas the minor signal did not decrease (*lane 8*). With OSGPEP'ase treatment, the signal detected with the anti-sLe^X and anti-CD43 mAbs disappeared completely (*lanes 6* and *10*). The size of gp135 was very close to that of CD43 (*lanes 5*, *7*, and *9*). These results suggest that gp135 is the major

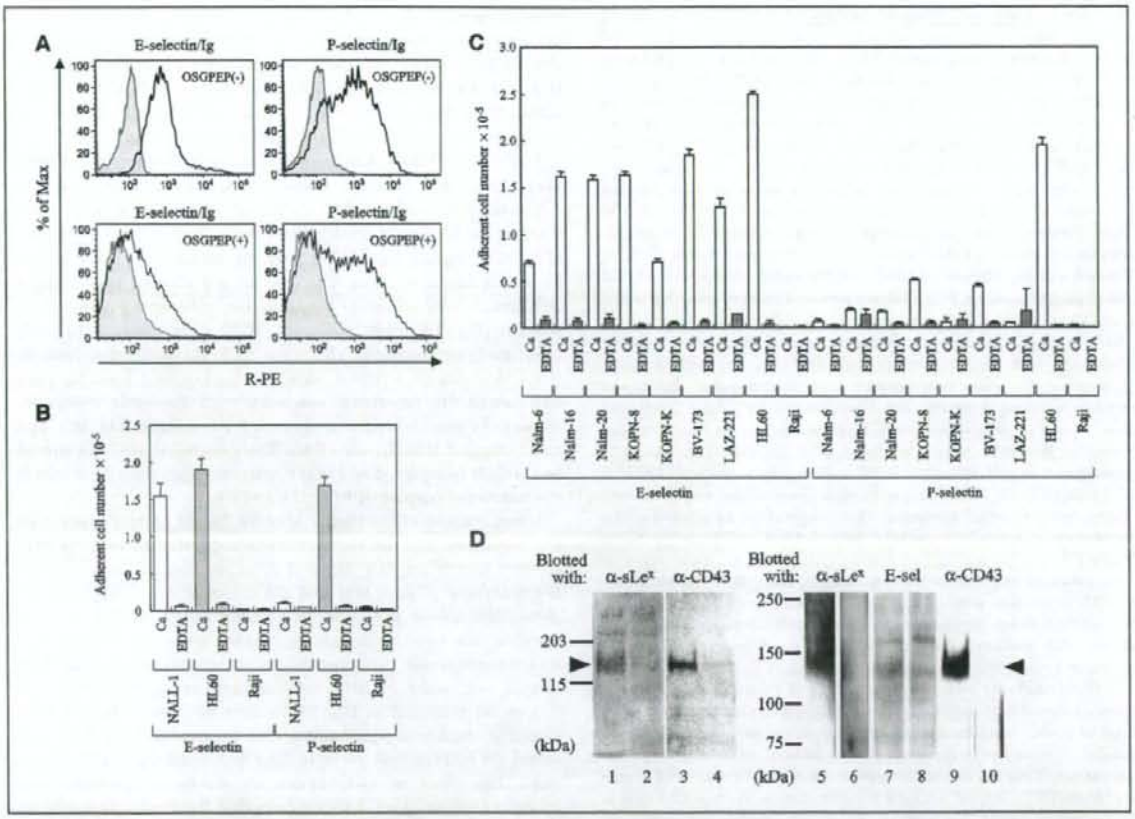

Figure 1. Reactivity with selectins on NALL-1 cells, low-shear-force cell adhesion assays of BCP-ALL cell lines, and analysis of the major E-selectin counter-receptor on NALL-1 cells. *A*, reactivity with E-selectin/P-selectin on NALL-1 cells pretreated with or without OSGPEP'ase. Cells were cultured in the presence or absence of OSGPEP'ase for 3 d, harvested, and subjected to flow cytometry. *Solid line*, the detection was carried out with human recombinant E-selectin or P-selectin in the presence of $CaCl_2$. *Gray shaded area*, reactivity in the presence of EDTA. *Top*, in the absence of OSGPEP'ase; *bottom*, in the presence of OSGPEP'ase. *B*, low-shear-force cell adhesion analysis of NALL-1 cells. Cells were labeled with BCECF-AM and incubated at 37°C for 30 min under low shear stress in well coated with selectin/Ig chimeric proteins. *White columns*, NALL-1; *gray columns*, HL60; *black columns*, Raji. *Ca*, in the buffer with $CaCl_2$; *EDTA*, in the buffer with EDTA. *Columns*, average cell number of three wells; *bars*, SD. *C*, low-shear-force cell adhesion analysis of the other BCP-ALL cell lines. Assay was carried out as above. *White columns*, in the presence of $CaCl_2$; *gray columns*, in the presence of EDTA. *Columns*, average cell number of three wells; *bars*, SD. *D*, Western and selectin blot analyses of NALL-1 cell lysate. *Left*, lysates of NALL-1 cells were subjected to 5.0% SDS-PAGE under reducing conditions and immunoblotted with anti-sLe^X mAb (CSLEX1; *lanes 1* and *2*) and with anti-CD43 mAb (DF-T1; *lanes 3* and *4*). The cell lysates were incubated with or without OSGPEP'ase and subjected to electrophoresis. *Lanes 1* and *3*, without OSGPEP'ase; *lanes 2* and *4*, with OSGPEP'ase. *Right*, NALL-1 cells were left untreated (*lanes 5*, *7*, and *9*) or pretreated with OSGPEP'ase during cell culture (*lanes 6*, *8*, and *10*). Cell lysates were subjected to 7.5% SDS-PAGE under reducing conditions and analyzed by Western blotting with anti-sLe^X mAb (CSLEX1; *lanes 5* and *6*), selectin blotting with E-selectin/Ig (*E-sel*; *lanes 7* and *8*), or Western blotting with anti-CD43 mAb (MEM59; *lanes 9* and *10*). *Left*, positions of molecular mass markers; *arrowheads*, positions of the signals.

carrier of E-selectin carbohydrate ligands in NALL-1 cells and that it may be CD43.

BCP-ALL cell lines express not PSGL-1 but CD43. PSGL-1 is known as a major ligand of P-selectin/E-selectin on neutrophils and subsets of T cells. Its molecular mass is similar to that of CD43 under reducing conditions (32), whereas it is ~250 kDa under nonreducing conditions. This is because PSGL-1 forms a disulfide-bonded homodimer. To discriminate CD43 from PSGL-1, we conducted SDS-PAGE under nonreducing conditions using the respective mAbs. PSGL-1 was clearly detected as a ~250-kDa band in HL60 cells but was not detectable in NALL-1 cells, which did not express detectable level of PSGL-1 (Fig. 2*A*, *top*). These cells were also analyzed with flow cytometry. As shown in Fig. 2*B*, PSGL-1 was not detected in NALL-1 (*top left*), whereas NALL-1 expressed CD43 (*top right*) and control HL60 expressed both PSGL-1 and CD43 (*bottom*). Next, we examined whether PSGL-1 and CD43 were present in the other BCP-ALL cell lines using flow cytometry. Nalm-6, Nalm-16, Nalm-20, KOPN-8, KOPN-K, BV-173, and LAZ221 were negative for PSGL-1 but strongly positive for CD43 (Table 1A, third and fourth columns). These results suggest that the major E-selectin ligand carrier is not PSGL-1 in BCP-ALL cell lines.

Clinical BCP-ALL samples are essentially PSGL-$1^{neg/low}$/CD43^{high}. To investigate whether primary B-precursor ALL cells and BCP-ALL cell lines shared the same characteristic expression of PSGL-1 and CD43, we performed a flow cytometric analysis of BM-derived leukemia cells from the 20 patients with BCP-ALL. For the expression of sialomucins, positivity for CD43 was >85% in 14 of 20 patients and >45% in 20 of 20 patients but PSGL-1 was negative

Table 1. Reactivity with selectin/Ig chimera and expression of sialomucins in BCP-ALL cell lines and BM-derived blast cells from patients with BCP-ALL

	E-selectin/Ig	P-selectin/Ig	PSGL-1	CD43	CD10
A					
Nalm-6	++	−	−	++++	++++
Nalm-16	+	++	−	++++	++++
Nalm-20	++	+++	−	++++	+++
KOPN-8	+++	++	−	+++	+++
KOPN-K	++	+++	−	+++	+++
BV-173	++	+++	−	+++	+++
LAZ221	++	+++	−	++++	+++
HL60	++++	++++	++++	++++	−
Raji	−	−	−	−	−
B					
Patient 1	++	++	±	++++	++++
Patient 2	++	+	−	++++	++++
Patient 3	++	++	+++	++++	−
Patient 4	++	++	+	++++	++++
Patient 5	n.t.	n.t.	±	++++	++++
Patient 6	n.t.	++	n.t.	++++	++++
Patient 7	++	+++	±	++++	+++
Patient 8	+	++++	±	++++	++++
Patient 9	+	+++	±	++++	+++
Patient 10	±	+++	±	++++	++++
Patient 11	+	+++	±	++++	±
Patient 12	n.t.	n.t.	+	++++	−
Patient 13	n.t.	n.t.	±	+++	++
Patient 14	n.t.	n.t.	±	+++	++++
Patient 15	n.t.	n.t.	±	++++	++++
Patient 16	n.t.	n.t.	±	++++	++++
Patient 17	+	+++	±	+++	++++
Patient 18	+	+++	±	++++	++++
Patient 19	n.t.	n.t.	±	+++	++++
Patient 20	+	+++	±	+++	++++

NOTE: A panel of BCP-ALL cell lines, HL60, and Raji cells were investigated for reactivity with selectin/Ig chimera and expression of CD43, PSGL-1, and CD10. BM-derived $CD45^+$ blasts were gated and stained with selectin/Ig chimeras and mAbs for CD43, PSGL-1, and CD10. The reactivity or expression was presented in a semiquantitative manner: ++++, >75% of cells positive; +++, 35% to 75% positive; ++, 15% to 35% positive; +, 5% to 15% positive; ±, 1% to 5% positive; −, <1% of cells positive.
Abbreviation: n.t., not tested.

to very weakly positive in 18 of 19 patients (Table 1B, third and fourth columns); most patients were PSGL-$1^{neg/low}$/$CD43^{high}$. The cells were PSGL-1^{high}/$CD43^{high}$ (Table 1B) in patient 3. They may have exceptional characteristics whose pathologic meaning is currently unclear. However, these results suggest that the majority of clinical BCP-ALL cells are PSGL-$1^{neg/low}$/$CD43^{high}$, and BCP-ALL cell lines, including NALL-1, essentially inherit characteristics of primary B-precursor ALL cells.

The major selectin ligand carrier protein gp135 is suggested to be CD43. To test whether gp135 is CD43 or not, we carried out coimmunoprecipitation and selectin pull-down assays. Figure 2*C* illustrates the results of the coimmunoprecipitation analysis. When the immunoprecipitation was performed with the anti-sLe^X mAb CSLEX1, a band with a molecular mass of ~135 kDa was detected along with additional signals for larger proteins (*lane 1*). The same immunoprecipitated sample clearly contained CD43 with a similar molecular size to gp135 (*lane 2*). In contrast, the immunoprecipitate obtained with anti-CD43 mAb was reactive not only with anti-CD43 but also with CSLEX1 at the same electrophoretic mobility (*lanes 3* and *4*). Figure 2*D* shows the result of an E-selectin pull-down analysis. The ~135-kDa signal was clearly detected by pull-down with E-selectin (*lane 2*). In contrast, control IgG could not pull-down any significant signal at ~135 kDa (*lane 4*). Although an additional ~220-kDa band was visualized (*lane 2*; *open arrowhead*), the signal was also detected with control IgG (*lane 4*) and thought to be nonspecific. To examine the presence of CD43 in the pull-down fractions, the proteins were released using EDTA from the selectin beads and again immunoprecipitated with anti-CD43 mAb. We could detect the ~135-kDa protein using anti-CD43 mAb (*lane 3*). These results suggest that the major selectin ligand carrier gp135 on NALL-1 cells is CD43.

Effect of CD43 knockdown on cell adhesion activity. The function of CD43 in cell adhesion was investigated in knockdown experiments. The knockdown efficiency of *CD43*-shRNA was 60% in NALL-1siCD43#1 and 49% in NALL-1siCD43#2 cells (Fig. 3*A*). CD43 expression was examined using flow cytometry and immunoblot

analyses (Fig. 3*B* and *C*). The mean fluorescence intensity (MFI) of CD43 in NALL-1siCD43#1 and NALL-1siCD43#2 was 7.6% and 65.2% of the control, respectively (Fig. 3*B*). As shown in Fig. 3*C*, the intensity of CD43 was markedly reduced in NALL-1siCD43#1 cells using the DF-T1 mAb (*lane 3*). CD43 expression in the NALL-1siCD43#2 subline was substantially diminished (*lane 4*). The reactivity with E-selectin/Ig was also evaluated using flow cytometry. Whereas MFI in NALL-1siCD43#2 cells was comparable with that in the parental cells, MFI in the NALL-1siCD43#1 subline decreased to 75% of the control (data not shown).

The effect of knocking down *CD43* was evaluated using functional low-shear-force cell adhesion assays (Fig. 4*A*). For adherence to E-selectin, the knockdown resulted in a 24% decrease in NALL-1siCD43#1 cells (*light gray columns*) and 7% decrease in NALL-1siCD43#2 cells (*striped columns*) compared with control NALL-1scrambled cells (*white columns*). Next, we conducted a rolling assay and the rolling activity of NALL-1 cells was evaluated on CHO-E cells. Under a constant shear stress of 5 dyne/cm^2, we detected significant NALL-1 cell rolling on CHO-E cells in the buffer containing $CaCl_2$ (Fig. 4*B* and *C*). Rolling events in NALL-1siCD43#1 and NALL-1siCD43#2 cells were significantly reduced (69% for #1 versus control, $P < 0.001$; 35% for #2 versus control, $P < 0.001$; Fig. 4*B*). For rolling velocity, knockdown of *CD43* resulted in a significant increase compared with the control (168% for #1 versus control, $P < 0.001$; 135% for #2 versus control, $P < 0.005$; Fig. 4*C*). These results suggest that CD43 on NALL-1 cells functions as an E-selectin ligand.

Down-regulation of CD43 inhibits tissue engraftment. Finally, we examined the effect of knocking down *CD43* on tissue migration using a mouse model. We chose NALL-1siCD43#1 cells for the cell migration assay *in vivo* using NOD/SCID mice. In the assay, parental NALL-1 cells essentially behaved like the NALL-1scrambled cells (Fig. 4*D*, *white columns*). We observed that more cells migrated to BM than those to spleen and liver at 6 h. Few cells were detected in peripheral blood. Migrated cells were also found at 24 h and their number was similar to that at 6 h. This observation suggested that the leukemic cells engraft to the peripheral lymphoid organs, not a simple transient migration. As shown in Fig. 4*D*, the migration/engraftment of the knockdown cells (*black columns*) decreased significantly compared with that of the scrambled cells (5–20%; *white columns*). The decrease at 24 h was similar to that at 6 h. To exclude any possible reduction in levels of other cell adhesion molecules by the knockdown, we examined the expression of

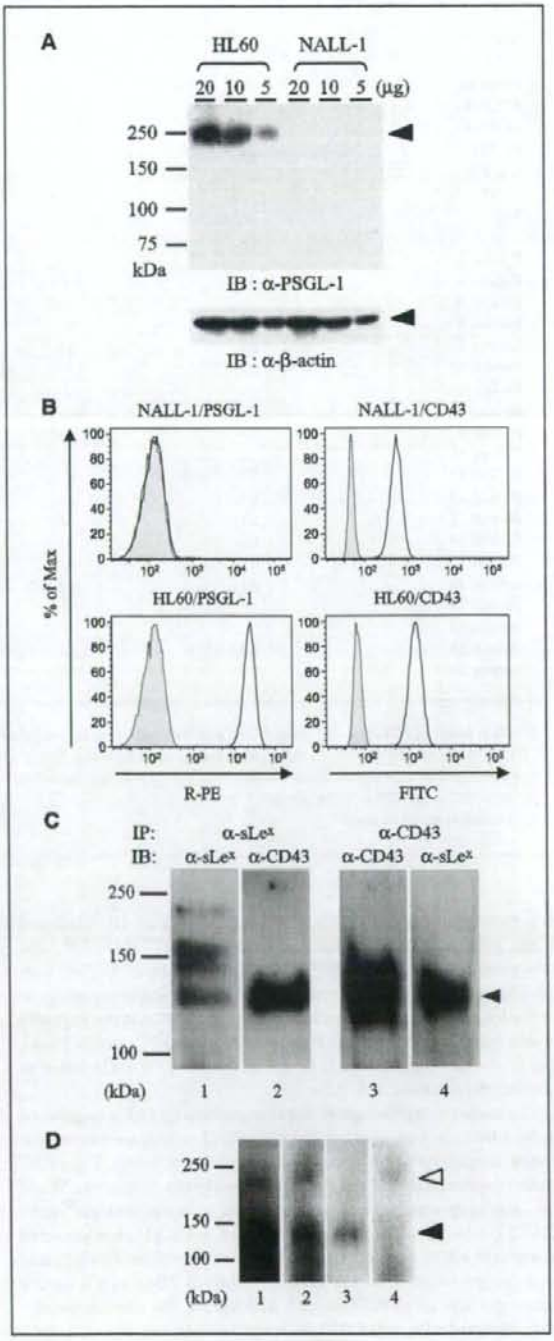

Figure 2. Expression of the E-selectin counter-receptor candidate in NALL-1 cells. *A*, lysates from NALL-1 and HL60 cells were subjected to SDS-PAGE under nonreducing conditions and immunoblotted with anti-PSGL-1 (KPL-1; *top*) or anti-β-actin (AC-15; *bottom*) antibody. *Left*, positions of molecular mass markers; *arrowheads*, positions of the signals. *B*, NALL-1 and HL60 cells were stained with anti-PSGL-1 and CD43 mAbs (KPL-1 and 1G10, respectively), and cell surface expression of sialomucin was detected using flow cytometry. *C*, coimmunoprecipitation of sLe^X carbohydrate antigen with CD43. NALL-1 cell lysates were immunoprecipitated (*IP*) with anti-sLe^X (CSLEX1; *lanes 1* and *2*) or anti-CD43 mAb (MEM59; *lanes 3* and *4*). Precipitates were subjected to SDS-PAGE under reducing conditions and immunoblotted (*IB*) with anti-sLe^X (CSLEX1; *lanes 1* and *4*) or anti-CD43 mAb (MEM59; *lanes 2* and *3*). *D*, selectin pull-down from cell lysates. NALL-1 cell surface proteins were biotinylated, subjected to SDS-PAGE under reducing conditions, and blotted with streptavidin-HRP and a chemiluminescence substrate. *Lane 1*, total lysate; *lane 2*, precipitates of the pull-down by E-selectin/Ig; *lane 4*, precipitates of the pull-down by control human IgG. *Lane 3*, to further show the pull-down of CD43 by selectins, precipitates obtained with E-selectin/Ig were released using EDTA and again precipitated with anti-CD43 mAb (MEM59). *C* and *D*, *closed arrowheads*, positions of the major carrier glycoprotein (gp135) and CD43; *left*, positions of molecular mass markers. *D*, *open arrowhead*, position of the nonspecific pull-down protein. *A* to *D*, data are representative of multiple independent experiments.